

Accepted Manuscript

Recognizing and quantifying metamorphosed alteration zones through amphibolite facies metamorphic overprint at the Key Anacon *Zn-Pb-Cu-Ag* deposits, Bathurst Mining Camp, New Brunswick, Canada

Joseph D.S. Zulu, David R. Lentz, James A. Walker, Christopher R.M. McFarlane

PII: S0375-6742(16)30039-5
DOI: doi: [10.1016/j.gexplo.2016.02.003](https://doi.org/10.1016/j.gexplo.2016.02.003)
Reference: GEXPLO 5702

To appear in: *Journal of Geochemical Exploration*

Received date: 29 December 2014
Revised date: 25 January 2016
Accepted date: 16 February 2016

Please cite this article as: Zulu, Joseph D.S., Lentz, David R., Walker, James A., McFarlane, Christopher R.M., Recognizing and quantifying metamorphosed alteration zones through amphibolite facies metamorphic overprint at the Key Anacon *Zn-Pb-Cu-Ag* deposits, Bathurst Mining Camp, New Brunswick, Canada, *Journal of Geochemical Exploration* (2016), doi: [10.1016/j.gexplo.2016.02.003](https://doi.org/10.1016/j.gexplo.2016.02.003)

This is a PDF file of an unedited manuscript that has been accepted for publication. As a service to our customers we are providing this early version of the manuscript. The manuscript will undergo copyediting, typesetting, and review of the resulting proof before it is published in its final form. Please note that during the production process errors may be discovered which could affect the content, and all legal disclaimers that apply to the journal pertain.



Recognizing and quantifying metamorphosed alteration zones through amphibolite facies metamorphic overprint at the Key Anacon Zn-Pb-Cu-Ag deposits, Bathurst Mining Camp, New Brunswick, Canada.

Joseph D.S. Zulu¹, David R. Lentz¹, James A. Walker² and Christopher R.M. McFarlane¹

¹Department of Earth Sciences, University of New Brunswick, Fredericton, New Brunswick Canada E3B 5A3 (d4ln8@unb.ca)

²Geological Surveys Branch, New Brunswick Department of Energy and Mines, P.O. Box 50, Bathurst, New Brunswick E2A 3Z1, Canada

ABSTRACT

The Key Anacon deposits, Bathurst Mining Camp, New Brunswick, are hosted in upper greenschist- to amphibolite-facies felsic volcanic rocks. The occurrence of cordierite-biotite and garnet-biotite-muscovite assemblages parallel to the regional tectonic fabric in the metamorphosed hydrothermal alteration zones point to a pre-metamorphic mineralization event that was synchronous with sub-aqueous volcanism. A combination of textural, mineralogical, lithochemical alteration indices and vectors, molar element ratios, and P - T diagrams have been used to recognize the effects of medium-grade metamorphism and establish the mass compositional changes associated with pre-metamorphic hydrothermal alteration. Modelling the altered felsic volcanic rocks in a K_2O - Fe_2O_3 - MgO - Al_2O_3 - SiO_2 - H_2O - TiO_2 (KFMASHT) system and comparing the observed peak metamorphic assemblages with those produced in a petrogenetic grid allows us to interpret the style of pre-metamorphic hydrothermal alteration related to deposit formation. The compositional change in the stratigraphic footwall (structural hanging wall) is characterized by mass gains of 0.1 to 4.0 wt. % Fe_2O_3 (Total), 0.7 to 22.2 wt. % MgO , and 0.5 to 55.2 wt. % CaO , and mass losses of 25.1 to 56.7 wt. % SiO_2 , 0.2 to 2.0 wt. % Na_2O , and 0.3 to 3.8 wt. % K_2O . Variable gains and losses of Zn, Pb, and Cu are characteristic of the footwall alteration zones with Zn displaying gains proximal to the sulfide lens, and losses distal to the massive sulfide lens. The alteration indices (AI) values increase as the massive sulfide lens is approached from either the footwall or hanging wall, whereas the Ghandi index (GI) discriminates the intensely chlorite-altered

rocks proximal to mineralization from the sericitic altered rock in more distal areas. Overall, there is an increase of the GI from the weakly to moderately altered zone (GI = 1.3 to 6.0) to the more intensely altered zone (GI = 6.1 and 60). Although the Chlorite-Carbonate-Pyrite index (CCPI) is similar to the GI, it is preferable to adopt the more robust GI, because it is a ratio of the added chemical components ($\text{Fe}_2\text{O}_3_{\text{(Total)}} + \text{MgO}$) to those lost from the system ($\text{Na}_2\text{O} + \text{K}_2\text{O}$) during the most intense hydrothermal alteration. These physical and geochemical observations are consistent with early feldspar-destructive alteration followed by chloritization proximal to the sulfide lens and accompanied by sericitization alteration distal prior to sulfidation and oxidation during prograde metamorphism.

Key words: Hydrothermal alteration, compositional change, Key Anacon, sulfidation and oxidation.

1. Introduction

The processes and hydrothermal fluids that form volcanogenic massive sulfide deposits are the same processes and fluids that give rise to alteration assemblages. Understanding the alteration processes has an economic significance in that it allows the geologist to use it as a vector toward the ore deposit. As mineralizing fluids migrate through the footwall stratigraphy some elements move from the host rocks into the fluid, whereas other elements move from the fluid phase and into the host rocks. This results in mass-gains and losses of the altered host rocks as the system is striving to attain chemical equilibrium (cf. Susak, 1994). Thus, the alteration assemblages develops the zone refining sequence that is controlled by the temperature, pressure, hydrothermal fluid composition, metal ion concentrations (mass action effect), relative stabilities of soluble complex ions, wall-rock interactions, multiple

hydrothermal fluxing and mixing, mineral free energies, and mineral volatilities (cf. Susak and Crerar, 1982).

Although VMS deposits are less likely to form at very high temperatures (primarily because high metal solubilities at high temperatures preclude the saturation of metals in hydrothermal fluids), many deposits including Key Anacon occur in metamorphic terranes up to and including amphibolite grade. To recognise these deposits, we need to be able to distinguish those that formed by metamorphic processes from those that were simply metamorphosed. In the case of the latter, we place the emphasis on seeing through the effects of metamorphism (McFarlane et al., 2007). Furthermore, because deposits in high grade metamorphic terranes contain few hydrous phases, identifying pre-metamorphic alteration may be the only way to explore for, or more importantly, understand these deposits. Spry (2000) demonstrated that the effects of sulfidation and oxidation on country rocks enclosing metamorphosed massive sulfide deposits constitute an exploration guide to ore. Sulfur and oxygen from the sulfide deposit react with the Fe component of ferromagnesian silicates (e.g., garnet, staurolite, chlorite, and biotite) or oxides (e.g., gahnite and högbomite) to produce Mg- or Zn-rich silicates or Zn-rich oxides with proximity to the ore (Spry and Scott, 1986; Spry, 2000). This halo of Mg-rich or Zn-rich minerals can be superimposed onto zones of pre-metamorphic alteration or can be developed around ore deposits where signs of alteration are apparently absent (Spry, 2000). The compositions of the resulting ferromagnesian silicates and Zn-rich minerals, as well as the distribution end-members of the system Ca-Ti-Fe-S-O, are dictated by the bulk-rock composition and by a variety of physicochemical conditions including T , P , fS_2 , fO_2 , and fH_2O . Therefore, sulfidation-oxidation haloes are most prominent where a large $fS_2 - fO_2$ gradient is apparent around an ore deposit. Furthermore, the presence of pyrrhotite, pyrite, and magnetite (high $fS_2 - fO_2$ conditions) in a metamorphosed massive sulfide body that is enveloped by graphite-bearing

(low fO_2 conditions) country rocks ensures such a gradient (cf. Spry, 2000). A consistent interpretation by Spry (2000) is that the proximity and abundance of graphite, in part, dictate the width of the sulfidation-oxidation halo to the massive sulfide body. Where graphite occurs adjacent to a sulfide body the halo will be narrow; however, if graphite occurs tens to hundreds of meters from sulfide mineralization, the likelihood of a wider halo is increased.

Recognizing and documenting the petrogenesis of alteration halos in metamorphic terrains is complicated by: 1) progressive metamorphic dehydration reactions that transform fine-grained hydrous alteration assemblages into medium-grained anhydrous assemblages; 2) mass-losses and gains that can change the bulk composition of the protolith; 3) sulfidation and oxidation reactions associated with the massive sulfide deposit may impart new diagnostic minerals that are stable under specific conditions, and/or restrict nucleation and growth of other mineral phases; 4) deformation may attenuate large alteration halos into parallelism with tectonic fabrics thereby obscuring the original geometry of the alteration envelopes. Therefore, quantification of the mass changes resulting from pre-metamorphic hydrothermal alteration is dependent on a combined understanding of the original bulk composition of the host rock prior to low temperature fluid-rock interactions, as well as the mineralogical and textural evolution of hydrothermal assemblages during prograde metamorphism.

The purpose of this paper is to characterize the pre-metamorphic chemical signature of the alteration assemblage from the metamorphic effects at the Key Anacon Zn-Pb-Cu-Ag deposit, located in the Bathurst Mining Camp, New Brunswick (Fig. 1). This deposit was deformed and metamorphosed at upper-greenschist to amphibolite facies conditions (400–570°C, 4.1±0.5 kbar) during the Palaeozoic (Zulu, 2012).

2. Geological Setting

The rocks of the Brunswick belt are assigned to two litho-stratigraphic groups, the Cambro-Ordovician Miramichi Group and Middle Ordovician Tetagouche Group (Skinner, 1974). The Miramichi Group is dominated by mature quartzose sedimentary sequence, which becomes progressively finer grained and more graphitic towards the contact with the Tetagouche Group rocks (van Staal and Williams, 1984; Lentz, 1996a). Rice and van Staal (1992) interpreted the graphitic phyllites and quartzose wackes as having been formed on an abyssal slope.

The Miramichi Group disconformably overlies the Miramichi Group and consists of Formations that, in ascending stratigraphic order are: Nepisiguit Falls, Flat Landing Brook, Little River, and Tomogonops formations. The Nepisiguit Falls Formation consists of quartz-feldspar-phyric felsic volcanic and associated sedimentary rocks. This formation has been interpreted as a pyroclastic sequence dominated by crystal-rich ash flow tuffs, reworked tuffites, and related sedimentary (van Staal et al., 1992). Volcanogenic massive sulphide deposits (e.g., Brunswick #12, Brunswick 6, and Key Anacon) and related Algoma-type iron formation occur at the top of the Nepisiguit Falls Formation.

In the eastern part of the Bathurst Mining Camp, the Nepisiguit Falls Formation is overlain by the Flat landing Brook Formation, which consists of feldspar-phyric to aphyric rhyolite flows, associated breccias and related hyalotuffaceous sedimentary rocks. However, at Key Anacon the Flat Landing Brook Formation is missing and mafic volcanic and related sedimentary rocks of the Little River Formation immediately overlie the massive sulfides and associated iron-formation (van Staal et al., 1992; Lentz and Langton, 1995).

The Little River Formation is overlain by carbonaceous shale and wacke of the Tomogonops Formation. The Tomogonops Formation is differentiated from the Miramichi Group by its locally more calcareous nature and less well developed penetrative fabric.

Five groups of folds are recognized. They can be divided unequivocally on the basis of overprinting, into four generations, but there are no known overprinting relationships between the two youngest groups (van Staal and Williams, 1984).

The thrust-related D_1 isoclinal (F_1) folds and associated axial planar schistosity (S_1) were progressively deformed into tight-to-isoclinal folds (F_2), resulting into S_1/S_2 transposition fabric, and are interpreted as high-strain deformation with F_1/F_2 fold interference structure (cf. van Staal and Williams, 1984). D_3 are recumbent and best developed in the west part of the BMC, and D_4 are represented as kink-folds in this area. The earliest folds (F_{1A} and F_{1B}) are tight to isoclinal and are related to coeval thrusting resulting from one progressive D_1 event.

3. Deposit stratigraphy

The Key Anacon Main Zone and the Key Anacon East Zone massive-sulfide deposits are approximately 15 km east-southeast of the Brunswick No. 12 mine and lies on the eastern limb of the large Portage River Anticline (Figs. 1 and 2). This autochthonous sequence consists of the Miramichi Group (argillite and quartzose-wacke) and the disconformably overlying Tetagouche Group. Here, the Tetagouche Group is divided into four formations that, in ascending stratigraphic order, are: Nepisiguit Falls (felsic volcanic rocks with associated sedimentary rocks), Little River (basalt, siltstone, and shale), and Tomogonops (grey locally calcareous wacke, siltstone and shale) formations.

The Nepisiguit Falls Formation (NF Fm) is the immediate footwall to the Key Anacon massive sulfide deposits and consists of and intercalated sequence of sedimentary rocks, ash, fine-grained quartz- and quartz-feldspar crystal tuff and volcanoclastic equivalents (Fig. 3a; Zulu, 2012). Towards the top of the NF Fm, enrichment of Zr in the volcanic epiclastic rocks is indicated by $Zr/TiO_2 \approx 0.13$, and is attributed to tectonic imbrication and intercalations of Miramichi Group quartzite(-pelite) with the NF Fm volcanic rocks.

The Key Anacon Main Zone and East Zone *Zn-Pb-Cu-Ag* massive sulfide deposits occur on the eastern limb of the large-scale Portage River Anticline (Figs. 1 and 2), and are localized in the hinges of parasitic F_2 folds. Five generations of folds have been recognized in the Key Anacon area (cf. van Staal and Williams, 1984; Irrinki, 1992; Zulu, 2012). The three earliest phases of folding have an important influence on the large-scale distribution of rocks units (Zulu, 2012). The main geometry of the massive sulfide folds are upright, isoclinal, and steeply plunging sheath-fold structures of the F_2 generation (Zulu, 2012).

4. Methodology

4.1. Lithogeochemical compositions

Under the conditions of hydrothermal alteration, such as those that must have prevailed in the volcanic host rocks (Fig. 3A-D) at the time the Key Anacon deposits formed, the major elements commonly used for rock type classification (e.g., Si, Na, and K) are highly mobile and consequently, unsuitable for protolith determination. In such cases, robust petrogenetically useful discrimination diagrams, based on elements that are immobile under hydrothermal conditions are used, i.e., the high-field-strength elements (HFSE), which include Al, Ga, Ti, Sc, Zr, Hf, Y, the heavy rare earth elements (HREE) Gd through to Lu, Th, and possibly Nb and Ta (Floyd and Winchester, 1978; Beswick and Soucie, 1978; Davies et al., 1979; Davies and Whitehead, 1980; Finlow-Bates and Stumpfl, 1981; Govett and Atherden, 1988; Ludden et al., 1982; Dostal and Strong, 1983; Leitch and Lentz, 1994; Lentz, 1999; Jenner, 1996).

Compiled whole-rock lithogeochemical data (Lentz, 1995; Lentz and Langton, 1995) were used to ascertain primary rock types and to document the effects of mineralization-related alteration processes. Fifty-two ($n=52$) representative felsic volcanic rock samples for the

purpose of mass-balance calculations (Table 1) were collected from drill cores from the Key Anacon deposit and include mafic volcanic rocks ($n=15$). Major elements analyses (Si, Ti, Al, Fe, Mg, Mn, Ca, Na, K, and P) were determined by X-ray fluorescence (XRF) spectrometry at four different laboratories (i.e., XRAL, now part of SGS Group, X-ray Assay laboratories of Don Mills, Ontario; Geological Survey of Canada; ACME Analytical laboratories, Vancouver, BC, and Activation Assay Laboratories, Ancaster, Ontario). The results of these compiled analyses ($n=200$) along with analytical methods and detection limits are tabulated in Zulu (2012). Rubidium, Sr, Y, and Zr at XRAL were determined by XRF of pressed powder pellets with a routine precision of 1 % for Rb and Sr (2 ppm and 1 ppm detection limits, respectively), 1 % for Y (1 ppm detection limit), and 2-3 % for Zr (10 ppm detection limit). Rare-earth elements (La, Ce, Pr, Nd, Sm, Eu, Gd, Tb, Dy, Ho, Er, Tm, Yb, and Lu) and trace elements were determined by inductively coupled plasma-mass spectrometry (ICP-MS). Detection limits are of the order of 0.1 ppm for La, Ce, Pr, Nd, Gd, Tb, Dy, Er, Tm, Yb, and Sm, and 0.05 ppm for Eu, Ho, and Lu.

4.2. Thermodynamic modelling of the metamorphosed alteration zone

Altered rock-specific equilibrium assemblage diagrams for the Key Anacon deposits were calculated using the model systems K_2O -FeO-MgO- Al_2O_3 - SiO_2 - H_2O - TiO_2 (KFMASHT), primarily because of the major cations present in chloritic and sericitic altered rocks are K_2O , FeO, MgO, Al_2O_3 , SiO_2 , and H_2O . In chlorite and sericite altered rocks both CaO and Na_2O tend to be easily mobilized and exert little influence on the overall mineral assemblage (Zulu, 2012). Consequently, modelling a primary alteration system using (KFMASHT) the metamorphic mineral assemblages developed in hydrothermal altered rocks can be easily predicted using petrogenetic grids and phase diagrams designed for shale or aluminous sedimentary rocks. These grids include thermodynamically calibrated systems, such as K_2O -

(FeO or MgO)-Al₂O₃-SiO₂-H₂O (KFASH, KMASH, KFMASH). Thermodynamic calculations were performed using the THERIAK-DOMINO software (de Capitani and Petrakakis, 2010), adopting a gridded Gibbs free-energy minimization approach (Connolly, 2005), and internally consistent and updated thermodynamic data set of Holland and Powell (1998). The results obtained for two representative samples are presented below.

5. Results

In terms of the Zr/TiO₂ versus Nb/Y discrimination diagram, felsic volcanic rocks assigned to the NF Fm in the footwall of both deposits for the most part plot in the rhyodacite field Zr/TiO₂ = 0.060 to 0.098; Fig 4), typical for this formation, whereas felsic volcanic rocks in the hanging wall at Key Anacon East Zone (FLB Fm) straddles the boundary between rhyolite and rhyodacite fields (Fig. 4A). However, some samples (n=13) of feldsparphyric volcanic and volcanoclastic rocks have more intermediate (andesitic to dacitic) compositions with Zr/TiO₂ contents of 0.020-0.030 (Fig 4). There is no known analogue in the Nepisiguit Falls Fm for rocks of this composition elsewhere in the Bathurst Mining Camp; therefore, it is suggested that they be included in a separate member or Formation. Most of the mafic volcanic rocks at the Key Anacon East Zone (n = 15), plot in the alkaline basalt field and two samples straddle the boundary between sub-alkaline basalt and alkaline basalt fields (Fig. 4A), and, one sample falls within the andesite field. In contrast, all mafic samples from the Key Anacon Main Zone plot in the alkaline basalt field (Fig. 4B).

Based on the Zr/TiO₂ versus Nb/Y classification, two chemostratigraphic units (rhyodacite-dacite, and dacite) have been recognized in the footwall rocks (NF Fm) at the Key Anacon Main Zone (Fig. 4B). The dacite and the rhyodacite-dacite together occupy the same stratigraphic position as the NF Fm (see Fig. 4B). The mixed felsic volcanic rocks fall in the andesite field (Fig 4B), whereas the dacite plot in the rhyodacitic-dacitic with Zr/TiO₂

contents that fall below 0.05 (Fig. 4B). Overall, the andesites have immobile trace-element characteristics that are similar to the rhyodacitic rocks of the NF Fm, except that their heavy-rare earth elements (HREE) and Y contents are lower (Zulu, 2012).

There are significant chemical differences between the footwall and hanging wall felsic volcanic rocks at the Key Anacon East Zone. Specifically, the higher Zr and lower TiO_2 in the hanging-wall (FLB Fm) relative to the footwall (Fig. 4A and 4B) reflects increased chemical evolution of the former (Lentz, 1996a). The Nb/Y value of < 0.8 is indicative of sub-alkaline composition (Fig. 4A and 4B), and is consistent with low Zr contents (100-250 ppm) in tuff units (Fig. 5).

The LR mafic rocks have a dominantly alkali to sub-alkaline basalt signature. The basalts have low Zr/TiO_2 (< 0.008) suggesting that Zr is incompatible during fractionation as it strongly partitions into the melt. In contrast, Ti, Cr, Ni, and V are high in the basalts due to presence of olivine, pyroxene, and hornblende (Fig. 5A and 5B).

The positive correlation between TiO_2 and Zr is also characteristic of alkali basalts, and is interpreted to reflect partial melting and fractionation from more mafic parent composition, as Zr and Ti are both incompatible in primitive melts. In contrast, Zr is strongly compatible in felsic melts as the fractionation proceeds from andesites through to rhyolite up to SiO_2 contents of 67 wt.%, whereupon Zr fractionates as zircon. The $\text{Y/Al}_2\text{O}_3$ - $\text{TiO}_2/\text{Al}_2\text{O}_3$ plots show distinct populations of the LR mafic rocks, and the NF and FLB felsic rocks (Fig. 5C and 5D).

The $\text{Zr/Al}_2\text{O}_3$ index is used to quantify the degree of alteration, with low values signifying mass loss and, high values for mass gain. The LR mafic rocks have only minor variation in Al_2O_3 content (12-16.4 wt %), which is compatible with the least-altered samples from the hanging-wall, whereas footwall felsic volcanic rocks have variation in Al_2O_3 content (11.5-22.1 wt %) suggesting strong alteration during chloritization (Zulu, 2012).

5.1. Host rock compositional changes in the Key Anacon deposits

In the footwall sequence of the Key Anacon Main Zone, deposit-related hydrothermal alteration (dominantly seawater) has resulted in a general mass increase in Fe_2O_3 (Total), MgO , and S^{T} , and mass loss of the alkali and the rare-earth elements. Contents of base metals (Zn, Pb, and Cu) increase in the footwall with proximity to the massive sulfide lens. The halos defined by the various mass changes extend into the footwall at least 130 m below the massive sulfide lens.

5.2. Compositional change

In order to quantitatively assess the effects of hydrothermal alteration, compositional change calculations were performed using the methodology of Barrett and MacLean (1994), and is as follows:

1. The calculation of an enrichment factor (EF), which is the ratio of Al_2O_3 content in the least-altered sample (precursor) to that of altered sample ($\text{EF} = \text{Al}_2\text{O}_3$ (precursor)/ Al_2O_3 (sample)). The least-altered composition used for calculations is that of the average Nepisiguit Falls Formation rhyodacite (Langton and McCutcheon, 1993).
2. The reconstructed composition (RC) for each altered sample is determined by multiplying the concentration (wt. % or ppm) of the elements by the correction factor CF (i.e., $\text{RC} = \text{EF} * \text{the concentration of major and trace elements in wt. \% and ppm, respectively}$).

Therefore, the compositional change or mass change (MC) for each chemical component is calculated by use of equation 1.1:

$$\text{MC}_i = \text{RC}_i - \text{PC}_i \dots \dots \dots (1.1)$$

Where; MC_i = compositional change (i), RC_i = concentration of element (i) in the reconstructed composition, and PC_i = concentration of element (i) in the least altered sample (precursor).

Down hole plots of the mass change for selected element along drill core KA92-10 shows a systematic variations in chemical components with respect to the footwall stratigraphy (Fig 7). Proximal footwall rocks (NF Fm) show minor mass loss of K_2O and Na_2O and major mass loss of SiO_2 (Fig. 7). Distal to the massive sulfide lens in the hanging wall, mass change diminishes to the expected values of the unaltered rhyodacite. Furthermore, a drastic reduction in MgO is observed as the massive sulfide lens is approached from both the hanging wall and footwall. Similarly, CaO , MnO , and Sr contents decrease towards the massive sulfide lens from both hanging wall and footwall (Fig. 7).

The calculated compositional changes in major-element oxides for 13 Samples from the NF Fm at the Key Anacon Main zone along section A-A', located on Fig 2, (see also DDH KA92-10; Fig. 8), are listed in Table 2. The compositional variation in the NF Fm of the stratigraphic footwall (structural hanging wall) is characterized by overall addition of $Fe_2O_{3(Total)}$, MgO , and S^T , and loss of SiO_2 , Na_2O , and K_2O (Fig. 7). These rocks have undergone mass gains of 0.1 to 4.0 wt. % $Fe_2O_{3(Total)}$, 0.7 to 22.2 wt. % MgO , and 0.5 to 55.2 wt. % CaO gains, and mass losses of 25.1 to 56.7 wt. % SiO_2 , 0.2 to 2.0 wt. % Na_2O , and 0.3 to 3.8 wt. % K_2O . Variable gains and losses of Zn , Pb , and Cu are characteristics of the footwall alteration zones with Zn gains proximal to the sulfide lens, and losses distal to the massive sulfide lens (Fig. 7). The mass changes of Zn range between -248 and 14254 ppm, whereas Pb has increased between 1.7 and 162 ppm (Table 2). The unit is also characterized by losses of Rb (52 to 126 ppm) and variable gains or losses in Sr and Ba (Table 2; Zulu, 2012). The net gain in FeO is highest in the core of the alteration zone, whereas the net gain in MgO is highest in the surrounding altered rocks (cordierite-biotite schists; cf. Franklin,

1997). Some cordierite-biotite bearing rocks have lower chlorite/sericite ratios, reflecting higher abundances of sericite at the margin of the alteration zone.

The mass changes related to hydrothermal alteration in the rocks hosting the Key Anacon deposits can be represented by the binary plots comparing compositional change of major elements (Fig. 8). Results in Figure 12 show that chloritization is the dominant alteration type affecting the rocks at the Key Anacon Main Zone. Primary chlorite alteration is metamorphosed to biotite and cordierite in the alteration zone (see Zulu, 2012). In most drill cores, the metamorphosed alteration halos are symmetrically distributed about the massive sulfide lenses (i.e., footwall and hanging wall alteration; cf. Wahl, 1977; Lentz, 1995; Lentz and Langton, 1995, Lentz, 1996a). However, asymmetrical alteration halos predominate in zones where sulfide concentration is localized within the F_2 parasitic folds, and is attributed to intense shearing coupled with strain partitioning in altered zones.

The net mass gains and losses in the altered volcanic rocks were calculated, based on the procedure of MacLean and Barrett (1993), and Barrett and MacLean (1994, 1999). The histogram of reconstructed mass changes for both gains and losses related to alteration of the host rocks are illustrated in Figure 9 and the calculated mass change for major oxides and selected trace elements are presented in Tables 2 and 3 (see also Zulu, 2012). For the purpose of this study the sample with zero mass change, i.e., the least-altered sample is sample 19 from drill hole KA92-5 @ 432.18 m. (Fig. 9).

5.3. Lithogeochemical Alteration Indices

Alteration indices (AI) were first proposed by Ishikawa et al. (1976), as a means to quantify the degree of alteration in volcanic rocks hosting the Kuroko-type VMS deposits. These authors proposed the AI ($AI = [(MgO + K_2O)] / [(MgO + Na_2O + K_2O + CaO)] * 100$) to assess the degree of sericite and chlorite alteration. This index encompasses reactions involving the breakdown of albite and volcanic glass (Na_2O and CaO loss) and their

replacement by sericite and chlorite (K_2O and MgO gain). The typical AI values for unaltered rocks lie between 20 and 60, whereas altered rocks commonly have AI values between 50 and 100, and rocks that have undergone complete replacement by sericite and/or chlorite having $AI = 100$. Häussinger et al. (1993) indicated that any index relating enriched and depleted elements can be equally useful in the estimation of the intensity of alteration; therefore, these authors calculated AI for the major (AI_{major}), and trace (AI_{trace}) elements separately, to improve the recognition of hydrothermal alteration. These AI_{major} versus AI_{trace} diagrams are sensitive to chemical variation related to hydrothermal alteration, and have been effectively employed in this study to document the degree of alteration. The reason for adopting this technique is as follows: during hydrothermal alteration, Fe_2O_3 (Total), MgO , and MnO are added, whereas Na_2O , and K_2O are lost (AI_{major}). Similarly, Zn , Cu , As , and Sn are added, whereas Sr , Ba , and rubidium are lost (AI_{trace}). The two AI equations are:

$$AI_{major} = (Fe_2O_3^T + MgO + MnO) / (Fe_2O_3^T + MgO + MnO + Na_2O + K_2O) \dots (1.2)$$

$$AI_{trace} = (Zn + Cu + As + Sn) / (Zn + Cu + As + Sn + Sr + Ba + Rb) \dots (1.3)$$

The AI_{major} index (generates values between 0 and 1) and is low (<0.24) in the least-altered rocks of the Bathurst Mining Camp (Lentz, 1996b). In contrast, higher values (close to 1) occur in the more intensely chloritized samples (Lentz, 1996b), whereas sericitized rocks have intermediate values (0.5-0.8; Fig. 10). The distinction between the least-altered, and sericitized or chloritized samples is clear and helps to discriminate the degree of alteration of the host rocks; thereby making it an effective and inexpensive vectoring tool. However, these diagrams should be restricted to felsic volcanic host rocks, such as the footwall rocks at the Key Anacon deposits, since mafic host rocks will return higher AI_{major} values, even when

unaltered (cf. Sánchez-España et al., 2000). Contrary to the compositional change evident on binary diagram (Fig. 8), the AI_{major} versus AI_{trace} diagram shows that the rocks in the Key Anacon Main Zone have experienced both chloritic and sericitic alteration (Fig. 10). This is consistent with field observations and thermodynamic modelling of metamorphosed alteration halo (see below).

The Gandhi index (GI) is another useful alteration index that has been successively employed in describing the type and intensity of chloritization of footwall rocks in the Bathurst Mining Camp (see Lentz, 1996b). The GI is calculated by equation 1.4:

$$GI = (Fe_2O_{3(\text{total})} + MgO)/(Na_2O + K_2O) \text{ or } GI = (Fe_{(\text{total})} + Mg)/(Na+K) \dots \dots \dots (1.4)$$

Lentz (1996b) observed that the GI is more robust than the AI since the ratio of the numerators and denominators are divergent ($\infty/-\infty$), whereas those of the AI approach unity ($0 \rightarrow 1$). In order to resolve the effects of carbonate alteration, Large et al. (2001) derived the Chlorite-Carbonate-Pyrite index (CCPI) that is defined by equation 1.5:

$$CCPI = \left[\frac{(FeO + MgO)}{(FeO + MgO + Na_2O + K_2O)} * 100 \right] \dots \dots \dots (1.5)$$

Down-hole plots of the AI, GI, and CCPI values for the samples collected from drill core KA92-10 were constructed to test the applicability of these alteration indices to the Key Anacon Main Zone (Figs. 11, 12; Table 3). This drill hole is collared in the stratigraphic footwall (structural hanging wall) and drilled toward the stratigraphic hanging wall and passes through the footwall alteration zone and sulfide lens, mafic rock of the hanging wall and then down section into the footwall (Fig. 12).

The AI values increase as the massive sulfide lens is approached from either the footwall or hanging wall. In contrast, the GI index discriminates the intensely altered chloritic zone, proximal to mineralization in the footwall from the more distal sericitic alteration (Figs. 11 and 12). Overall, there is an increase of the GI values from the weakly to moderately altered

zone (GI = 1.30 and 6.04) to the more intensely altered zone (GI = 6.08 and 60; Table 3; Zulu, 2012). Although the down-hole plot of CCPI is similar to that of the GI, it is preferable to adopt the more robust GI, because it is a ratio of the added chemical components ($\text{Fe}_2\text{O}_3_{(\text{Total})} + \text{MgO}$) to those lost from the system ($\text{Na}_2\text{O} + \text{K}_2\text{O}$) during the most intense hydrothermal alteration.

5.4. Molar Element Ratio Analysis

Molar Element Ratio (MER) analysis is a viable alternative to further refine the relationship between alteration-related, major-element lithogeochemical variations and alteration mineral assemblages (Madeisky and Stanley, 1993). Molar Element Ratio (MER) analysis of data collected from NF Fm rocks in drill hole KA92-10 clearly demonstrates the relationship between major-element lithogeochemical variations and the mineral assemblage in the alteration zones. For this purpose, the Na, K, Mg, and Fe versus Al are effective for displaying mineralogical composition of altered and unaltered rhyolites and rhyodacites plots (Figs. 13 and 14) (cf. Davies and Whitehead, 2006).

These plots show that chlorite and sericite (or muscovite) is the two main alteration minerals exerting control on the variation of Na_2O and K_2O . The alkali-alumina MER diagram clearly shows a negative correlation between Na/Al and K/Al for sericite-altered rocks, and clearly demonstrates that chlorite is the dominant alteration mineral within the NF Fm rocks intersected by drill hole KA92-10 (Fig. 13A). Most samples from the stratigraphic footwall are dominated by chloritic alteration, which is common in highly altered footwall rocks hosting VMS deposits (Lentz, 1996b), whereas the hanging wall rocks are dominated by sericitic alteration (Fig. 13A). The MER discrimination diagrams show that the degree of alteration increases with decreasing Na/Al within the albite-chlorite-muscovite field (i.e., the epidote-chlorite field of Davies and Whitehead, 2006), and is attributed to proximal-type chlorite \pm sericite development during feldspar destructive hydrothermal alteration.

In contrast, the Fe/Al versus Mg/Al discrimination diagrams shows that the variation in Fe_2O_3 (Total) and MgO is controlled by Fe-rich chlorite, Mg-rich chlorite, and pyrite (Fig. 13B). This diagram reveals that an increase in the Fe/Al of Fe-rich chloritic samples occurs at the expense of low Mg/Al in samples dominated by Mg-rich chlorites.

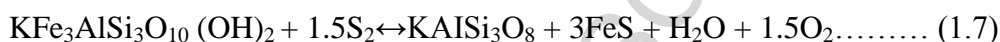
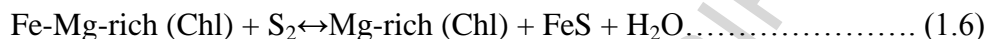
Similarly, Molar Element Ratio plots of Fe/Al versus K/Al and Mg/Al versus K/Al show that early, low-temperature chlorite alteration in areas distal to the sulfide lens, is overprinted by later intense high-temperature footwall alteration (Fig. 14A). The proximal-type alteration is characterized by Fe-rich chlorite, whereas the distal low-temperature alteration zone is dominated by high Mg-chlorite that locally contains talc and carbonate (Fig. 14B). The distal-type alteration is characterized by feldspar destruction and increasing FeO+MgO to form sericitic alteration zones.

5.5. Metamorphosed alteration zone

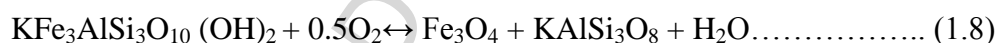
It has been demonstrated in this study that two types of deposit-related hydrothermal alteration likely affected the footwall rocks at the Key Anacon deposits, namely: chloritic (+Mg,+Fe,-Ca,-Na,-K), and sericitic (+K,+Mg, \pm Fe,-Ca,-Na), prior to regional metamorphism (see Zulu, 2012). Most samples from the chloritic and sericitic alteration zones have undergone mass loss resulting in apparent enrichment of immobile element contents (Fig. 6). At the upper greenschist- to amphibolites-grade metamorphism reached at Key Anacon the original hydrothermal alteration facies, i.e., Mg-rich chlorite \pm talc \pm sericite \pm quartz and sericite \pm chlorite \pm quartz, are characterized by the cordierite-biotite bearing, and garnet-bearing (garnet+chlorite+phengite+biotite+quartz) assemblages, respectively (Zulu, 2012).

The alteration host-rock silicate assemblage around the massive sulfide deposits is commonly overprinted by sulfur-bearing fluids during metamorphism, and is characterized by sulfidation and oxidation reactions (cf. Spry, 2000). For the Key Anacon deposits,

pyrrhotite, pyrite, and magnetite appear to be the reaction products that are produced by destabilization of Fe-Mg-silicates. Two such reactions that may have taken place and involving chlorite and biotite, respectively, are (1.6) and (1.7):



Magnetite is produced during prograde metamorphic conditions when the system has low sulfur fugacity ($f\text{S}_2$) and high oxygen fugacity ($f\text{O}_2$), resulting in reaction 1.8):



Combining reactions (1.7) and (1.8) during sulfidation, yields the important equilibrium relation between magnetite and pyrrhotite, i.e., reaction (1.9):



In reactions (1.6) to (1.8), the iron component of chlorite and biotite breaks down upon reacting with the vapour phases to form Mg-enriched chlorite and biotite, at the expense of pyrrhotite and magnetite. Despite high iron contents in the bulk-rock composition, the formation of abundant pyrrhotite around the Key Anacon deposits may have restricted nucleation and growth of staurolite (Zulu, 2012); however, modelling of the alteration halos did not take into account of the presence of sulfide phases.

Modeling of the chlorite alteration zone in drill core KA92-10 @ 726 m, in the KFMASHT system ($\text{SiO}_2\text{-Al}_2\text{O}_3\text{-(FeO or MgO)-K}_2\text{O-H}_2\text{O-TiO}_2$), as a function of pressure (maximum of 4.1 kbar calculated from different barometers; Zulu, 2012) and temperature is shown in Figure 15. The altered volcanic rocks are metamorphosed to a low-grade mineral assemblage dominated by chlorite, phengite, ilmenite, rutile, and quartz (Stage 1; Fig. 15). These rocks are enriched in Al, Fe, Mg, Ca, and K, and depleted in Si, Ti, and Na suggesting some calcic or sodic hydrothermal alteration. During prograde metamorphism (Stage 2; Fig. 15), chlorite in the chloritic alteration zone ($\text{Si+Al+Mg+Fe}\pm\text{K}$) breaks down to chlorite and biotite and subsequently andalusite at pressures below 3.0 kbar, in both cases forming metamorphic quartz as a product.

The petrogenetic grids for the KFMASHT system indicates that phengite, biotite, and quartz are produced from the breakdown of excess chlorite and sericite at temperatures above 425°C (stage 2; Fig. 15), consistent with the calibrated KFMAS system of Wang et al. (1986) and Trägårdh (1991). Peak metamorphic assemblage of amphibolite facies conditions for sample KA92-10 @ 720 m, occurs when destabilization of chlorite, phengite, and aluminosilicate results in an assemblage dominated by cordierite+biotite (Crd+Bt) at 3.0 kbar and temperature window of $570\text{-}600^\circ\text{C}$ (stage 3; Fig. 15). This metamorphic assemblage is consistent with petrographic analysis and indicates that a pre-metamorphic K and Mg enrichment attributed to chlorite-sericite alteration proximal to the massive sulfide lenses, affected the footwall rocks (Zulu, 2012).

Sericitic alteration (Si, Al, K, and Fe or Mg) metamorphosed at low grade, consists mainly of sericite, quartz, and sulfide minerals. These minerals are destabilized during prograde metamorphism (i.e., up to 3.5 kbar and $< 350^\circ\text{C}$) to form chlorite, phengite, microcline, pyrophanite, pyroxmangite, biotite, and quartz (Fig. 16; stage 1). At amphibolite facies conditions, pyrophanite, pyroxmangite, microcline, and partly chlorite are consumed in the

garnet-forming reaction, with the remaining chlorite, phengite, and biotite changing chemical composition (Fig. 16; stage 2). The equilibrium mineral assemblage in sample KA92-40 @ 669.2 m (94-DL-87) is consistent with results predicted from the forward modelling of the metamorphic peak assemblage. These rocks are interpreted to reflect sericitic alteration of felsic volcanic rocks, metamorphosed at upper greenschist (Fig. 16; stage 2) to amphibolite facies (Fig. 16; stage 3). The mid-upper amphibolite facies conditions represented in shales (e.g., sample BR11-670 m in Zulu, 2012) by an assemblage of $\text{Ilm} + \text{Grt} \pm \text{Phg} + \text{Bt} + \text{Crd}$ (mineral abbreviations from Kretz, 1983) are missing in the altered felsic volcanic rocks, suggesting that peak metamorphic conditions were lower amphibolite facies (see Fig. 16; stage 3). These metamorphic assemblages are interpreted to reflect intense primary metasomatic hydrothermal alteration of felsic host rocks. Recognition of this primary assemblage is a useful guide in exploring for VMS deposits in medium- to high-grade metamorphic terranes (cf. Franklin, 1997; Vernon and Clarke, 2008).

6. DISCUSSION AND CONCLUSION

In poly-deformed medium- to high-grade metamorphic terranes, well developed hydrothermal alteration zones associated with VMS deposits, such as those along the Brunswick Belt (Lentz, 1999), including the two Key Anacon deposits, can be readily recognized thereby providing important vectors to ore. Metamorphism of hydrothermal alteration zones gives rise to diagnostic, mineral assemblages. For example, the cordierite-biotite (K-bearing) rocks around the massive sulfide deposits, likely formed by metamorphism of a primary $\text{Chl} \pm \text{Mus} \pm \text{Tlc} \pm \text{Qtz}$ alteration assemblages (Zulu, 2012). In contrast, the garnet-chlorite-phengite-biotite bearing rocks likely formed by metamorphism of a primary sericite \pm chlorite + quartz alteration assemblage. The mineral assemblages determined from forward modelling of these altered felsic volcanic rocks are consistent with

petrographically recognizable mineral assemblages. Therefore, mapping and recognition of metamorphosed alteration zones provides constraints on the intensity and the spatial distribution of hydrothermal systems, targets for systematic lithogeochemical and geophysical exploration, and supportive evidence for metallogenic models.

Hydrothermal alteration that is chemically distinct from the typical host rocks can be recognized with a reasonable degree of confidence during the course of regional mapping as long as it is not confused with volumetrically insignificant footwall units, i.e. sedimentary rocks. Follow-up lithogeochemistry using alteration indices (Ishikawa et al., 1976; Häussinger et al., 1993; Hodges and Manojlovic, 1993; Large et al., 2001; Piché and Jébrak, 2004) or mass-balances techniques (MacLean and Kranidiotis, 1987; MacLean, 1988; MacLean and Barrett, 1993; Leitch and Lentz, 1994) are helpful in refining field interpretations.

Molar Element Ratio plots of Na/Al versus K/Al, Fe/Al versus K/Al, Mg/Al versus K/Al, and Fe/Al versus Mg/Al (Figs. 13 and 14) demonstrate that the alteration of the volcanic rocks in the Key Anacon deposits were controlled by the formation of sericite (muscovite) and Mg-chlorite from low-temperature hydrothermal fluids, and Fe-chlorite, and pyrite from high-temperature hydrothermal fluids.

The mass changes and down-hole plots of compositional variations are marked by large SiO₂ losses (Table 2; from Zulu, 2012) and systematic variation in the whole rock geochemistry (Fig. 7). Potassium was added to most altered rocks during VMS formation but may have been leached from the cordierite-biotite rock. The alteration zones lost CaO, Na₂O, Ba, Sr, and gained MgO, Fe₂O_{3 (Total)}, MnO, Pb, and Rb (Fig. 7). The net gain in Fe₂O_{3 (Total)} in footwall rocks was highest in the core of the alteration zone (see Zulu, 2012), whereas the net gain of MgO was highest in areas peripheral to the Fe-rich core (cordierite-biotite rocks).

Down-hole plots of three alteration indices for drill hole KA92-10 at the Key Anacon Main Zone demonstrates that the Gandhi (GI) index is the best vector for identifying mineralization. However, other alteration indices such as the AI are robust and are also useful indices for mineral exploration. The GI index and the Chlorite-Carbonate-Pyrite index (CCPI) are similar (Fig. 11); however the GI index is preferred as it is defined by the ratio of added components ($\text{Fe}_2\text{O}_3_{(\text{Total})} + \text{MgO}$) to the leached ($\text{Na}_2\text{O} + \text{K}_2\text{O}$) components.

ACKNOWLEDGEMENTS

This project is part of a Ph.D thesis to the first author and has been supported by the NB DNR grant to David Lentz and NSERC Discovery grants to both David Lentz and Christopher McFarlane. Dr. Steve McCutcheon is thanked for discussion on the geology of Bathurst Mining Camp.

References

- Barrett, T.J., and MacLean, W.H., 1994. Chemostratigraphy and hydrothermal alteration in exploration for VHMS deposits in greenstones and younger volcanic rocks: Geological Association of Canada, Short Course Notes 11, p.433-467.
- Barrett, T.J., and MacLean, W.H., 1999. Volcanic sequences, lithogeochemistry, and hydrothermal alteration in some bimodal volcanic-associated massive sulfide systems: Volcanic-associated massive sulfide deposits; processes and examples in modern and ancient settings: *Reviews in Economic Geology*, v.8, p.101-131.
- Beswick, A.E., and Soucie, G., 1978. A correction procedure for metasomatism in an Archean Greenstone Belt: *Precambrian Research*, 6, p.235-248.
- Connolly, J.A.D., 2005. Computation of phase equilibria by linear programming: a tool for geodynamic modeling and its application to subduction zone decarbonation: *Earth and Planetary Science Letters*, v.204, p.61-74.
- Davies, J.F., Grant, R.W.E., and Whitehead, R.E.S., 1979. Immobile trace elements and Archean volcanic stratigraphy in the Timmins area, Ontario: *Canadian Journal of Earth Sciences*, v.16, p.305-311.
- Davies, J.F., and Whitehead, R.E.S., 1980. Further immobile element data from altered volcanic rocks, Timmins area, Ontario: *Canadian Journal of Earth Sciences*, v.17, p.419-423.
- Davies, J.F., and Whitehead, R.E., 2006. Alkali-alumina and MgO-alumina Molar Ratios of altered and unaltered rhyolites: *Exploration and Mining Geology*, v.15, Nos. 1-2, p.75-88.
- de Capitani, C., and Petrakakis, K., 2010. The computation of equilibrium assemblage diagrams with Theriak/Domino software: *American Mineralogist*, v.95, no. 7, p.1006-1016: 10.2138/am.2010.3354.

- Dostal, J., and Strong, D.F., 1983. Trace-element mobility during low-grade metamorphism and silicification of basaltic rocks from Saint John, New Brunswick: *Canadian Journal of Earth Sciences*, v.20, p.431-435.
- Finlow-Bates, T., and Stumpfl, E.F., 1981. The behaviour of so-called immobile elements in hydrothermally altered rocks associated with volcanogenic submarine-exhalative ore deposits: *Mineralium Deposita*, v.16, p.319-328.
- Floyd, P.A., and Winchester, J.A., 1978. Identification and discrimination of altered and metamorphosed volcanic rocks using immobile elements: *Chemical Geology*, v.21, p. 291-306.
- Franklin, J.M., 1997. Lithogeochemical and Mineralogical Methods for Base Metal and Gold Exploration. In: Gubins (editor), "Proceedings of Exploration 97: Fourth Decennial International Conference on Mineral Exploration", p.191–208.
- Govett, G.J.S., and Atherden, P.R., 1988. Applications of rock geochemistry to productive plutons and volcanic sequences: *Journal of Geochemical Exploration*, v.30, p. 223-242.
- Häussinger, H., Okrusch, M., and Scheepers, D., 1993. Geochemistry of premetamorphic hydrothermal alteration of metasedimentary rocks associated with the Gorob massive sulphide prospect, Damara Orogen, Namibia: *ECONOMIC GEOLOGY*, v.88, p.72-90.
- Hodges, D.J., and Manojlovic, P.M., 1993. Application of Lithogeochemistry to exploration for deep VMS deposits in high-grade metamorphic rocks, Snow Lake, Manitoba: *Journal of Geochemical Exploration*, v.48, p.201-224.
- Holland, T.J.B., and Powell, R., 1998. An internally-consistent thermodynamic data set for phases of petrological interest: *Journal of Metamorphic Geology*, v.16, p.309-343.
- Irrinki, R.R., 1992. Key Anacon sulfide deposit, Gloucester County, New Brunswick: *Exploration and Mining Geology*, v.1, p.121-129.
- Ishikawa, Y., Sawaguchi, T., Iwaya, S., Horiuchi, M., 1976. Delineation of prospecting targets for Kuroko deposits based on modes of volcanism of underlying dacites and alteration haloes: *Mining Geology*, v.26, p.105-117.
- Jenner, G.A., 1996. Trace element geochemistry of igneous rocks: Geochemical nomenclature and analytical geochemistry. In: Wyman, D.A. (editor), Trace element geochemistry of volcanic rocks: Application for massive sulphide exploration: Geological Association of Canada, Short Course Notes, v.12, p.51-78.
- Kretz, R., 1983. Symbols for rock-forming minerals: *American Mineralogist*, v.68, p.277-279.
- Langton, J.P., and McCutcheon, S.R., 1993. Brunswick Project, NTS 21 P/5 West, 21 P/4 West, Gloucester County, New Brunswick: In: Abbott, S.A. (editor). New Brunswick Department of Natural Resources and Energy, Mineral Resources, Information Circular 93-1, p.31-51.
- Large, R.R., Gemmel, J.B., and Paulick, H., 2001. The alteration box plot: a simple approach to understanding the relationship between alteration mineralogy and lithogeochemistry associated with volcanic-hosted massive sulphide deposits: *ECONOMIC GEOLOGY*, v.96, p.957-971.
- Leitch, C.H.B., and Lentz, D.R., 1994. The Gresens approach to mass balance constraints of alteration systems: methods, pitfalls, examples. In: Lentz, D.R. (editor), Alteration and alteration processes associated with Ore-forming systems: Geological Association of Canada, Short Course Notes 11, p.161-192.
- Lentz, D.R., 1995. Stratigraphy and structure of the Key Anacon massive-sulphide deposits compared with the Brunswick deposits, Bathurst Mining Camp, New Brunswick. In: Langton, J.P. (editor), New Brunswick Department of Natural Resources and Energy,

- Minerals and Energy Division, Geoscience Research 1994, Miscellaneous Report 15, p.23-44.
- Lentz, D.R. and Langton, J.P. 1995. Key Anacon East Zone massive sulphide deposit: a new discovery in the Bathurst Mining Camp, New Brunswick: PDA Abstract volume, Toronto, Ontario, 10 p.
- Lentz, D.R. 1996a. Trace-element systematics of felsic volcanic rocks associated with massive-sulphide deposits in the Bathurst Mining Camp: petrogenetic, tectonic and chemostratigraphic implications for VMS exploration. In: Wyman, D.A. (editor), Trace Element Geochemistry of Volcanic Rocks: Applications for Massive Sulphide Exploration: *Geological Association of Canada, short course Notes*, 12, p.359-402.
- Lentz, D.R., 1996b. Recent advances in Lithochemical Exploration for massive-sulphide deposits in volcano-sedimentary environments: Petrogenetic, Chemostratigraphic, and alteration aspects with examples from the Bathurst Camp, New Brunswick. In: Current research, Carroll, B.M.W. (editor), New Brunswick Department of Natural Resources and Energy, Minerals and Energy Division, Mineral Resource Report 96-1, p.73-119.
- Lentz, D.R., 1999. Petrology, geochemistry, and oxygen isotope interpretation of felsic volcanic and related rocks hosting the Brunswick No. 6 and No. 12 massive sulfide deposits, Bathurst Mining Camp, Canada: *ECONOMIC GEOLOGY*, v.94, p.57-86.
- Ludden, J., Gelinás, L., and Trudel, P., 1982. Archean metavolcanics from the Rouyn-Noranda district, Abitibi greenstone belt, Quebec. 2. Mobility of trace elements and petrogenetic constraints: *Canadian Journal of Earth Sciences*, v.19, p.2276-2287.
- MacLean, W.H., 1988. Rare earth element mobility at constant inter-REE ratios in the alteration zone at the Phelps Dodge massive sulphide deposit, Matagami, Quebec: *Mineralium Deposita*, v.23, p.231-238.
- MacLean, W.H., and Barrett, T.J., 1993. Lithochemical techniques using immobile elements: *Journal of Exploration Geochemistry*, v.48, p.109-133.
- MacLean, W.H., and Kranidiotis, P., 1987. Immobile elements as monitors of mass transfer in hydrothermal alteration: Phelps Dodge massive sulfide deposit, Matagami, Quebec: *ECONOMIC GEOLOGY*, v.82, p.951-962.
- Madiesky, H.E., and Stanley, C.R., 1993. Lithochemical exploration of metasomatic zones associated with volcanic-hosted massive sulfide deposits using Pearce Element Ratio analysis: *International Geology Review*, v.35, p.1121-1148.
- McFarlane, C.R.M., Mavrogenes, J.A., and Tomkins, A.G., 2007. Recognizing hydrothermal alteration through a granulite facies metamorphic overprint at the challenger Au deposit, South Australia: *Chemical Geology*, v. 243, p. 64–89.
- Piché, M., and Jébrak, M., 2004. Normative minerals and alteration indices developed for mineral exploration: *Journal of Geochemical Exploration*, v.82, p.59-77.
- Rice, R.J. and van Staal, C.R., 1992. Sedimentological Studies in the Ordovician Miramichi, Tetagouche, and Fournier groups in the Bathurst camp and the Belledune-Elmtree Inlier, northern New Brunswick: In *Current Research, Geological Survey of Canada, Paper 92-1D*, p.257-264.
- Sánchez-España, J., Velasco, F., and Yusta, I., 2000. Hydrothermal alteration of felsic volcanic rocks associated with massive sulphide deposition in the northern Iberian Pyrite Belt (SW Spain): *Applied Geochemistry*, v.15, p.1265-1290.
- Skinner, R., 1974. Geology of the Tetagouche Lakes, Bathurst, and Nepisiguit Falls map-areas, New Brunswick with emphasis on the Tetagouche Group: *Geological Survey of Canada Memoir 371*, 133 p.
- Spry, P.G., and Scott, S.D., 1986. Zincian Spinel and Staurolite as Guides to Ore in the Appalachians and Scandinavian Caledonides. *Canadian Mineralogist*, v. 24, p. 147-163.

- Spry, P. G., 2000. Sulfidation and Oxidation Haloes as Guides in the Exploration for Metamorphosed Massive Sulfide Ores. In: Spry, P.G., Marshall, B. and Vokes, F.M. (Editors), *Metamorphosed and Metamorphogenic Ore Deposits*. *Economic Geol. Rev.*, v.11: p. 149-161.
- Susak, N.J., and Crerar, D.A., 1982. Factors Controlling Mineral Zoning in Hydrothermal Ore Deposits: *ECONOMIC GEOLOGY*, v.77, p.476-482.
- Susak, N.J., 1994. Alteration Factors affecting Ore Deposition: In: Lentz, D.R. (editor), *Alteration and Alteration Processes Associated with Ore-Forming Systems: Geological Association of Canada, Short Course Notes*, v.11, p.69-99.
- Trägårdh, J., 1991. Metamorphism of magnesium-altered felsic volcanic rocks from Berglagen, central Sweden: A transition from Mg-chlorite- to cordierite-rich rocks: *Ore Geology Reviews*, v.6, p.485-497.
- van Staal, C.R., and Williams, P.F., 1984. Structure, origin and concentration of the Brunswick 12 and 6 orebodies: *ECONOMIC GEOLOGY*, v.79, p.1669-1692.
- van Staal, C.R., Fyffe, L.R., Langton, J.P. and McCutcheon, S.R., 1992. The Ordovician Tetagouche Group, Bathurst Camp, northern New Brunswick, Canada: history, tectonic setting, and distribution of massive-sulphide deposits: *Exploration and Mining Geology*, **1**, 93-103.
- Vernon, R.H., and Clarke, G.L., 2008. *Principles of Metamorphic Petrology*: Cambridge University Press, New York, U.S.A., 446p.
- Wang, G.-F., Banno, S., and Tackeushi, K., 1986. Reactions to define the biotite isograd in the Ryoke metamorphic belt, kii Peninsula, Japan: *Contributions to Mineralogy and Petrology*, v.93, p.9-17.
- Wahl, J.L., 1977, Rock geochemical exploration at the Heath Steele and Key Anacon deposits, New Brunswick: Unpublished Ph.D. thesis, University of New Brunswick, Fredericton, New Brunswick, 429 p.
- Winchester, J.A., and Floyd, P.A., 1977. Geochemical discrimination of different magma series and their differentiation products using immobile elements: *Chemical Geology*, v.20, p.325-343.
- Zulu, J.D.S., 2012. Deformation and metamorphism of the Key Anacon Zn-Pb-Cu-Ag deposits, Bathurst Mining Camp, New Brunswick, Canada. Unpublished Ph.D. thesis, Fredericton, New Brunswick, *University of New Brunswick*, 576 p.

Figure Caption

Figure 1: A Geological map of eastern part of the Bathurst Mining Camp showing location of the Key Anacon, Brunswick No. 12 and No.6 deposits, New Brunswick, Canada (modified after van Staal and Williams, 1984). Detailed geology of the Key Anacon are presented in Figure 2.

Figure 2. Geological map showing the position of the Key Anacon Main and Key Anacon East deposits (stars) and the Legere Cu occurrence (red circle), and a section through A-A', Bathurst Mining Camp, New Brunswick (Canada). Black dashed-lines are faults. Note: east of the dotted line Cambro-Ordovician rocks are covered by the carboniferous. Area of Figure is outlined on Figure 1.

Figure 3. Photographs of rocks from the Key Anacon deposit **A)** Nepisiguit Falls Formation felsic crystal tuff with medium-grained feldspar-quartz crystals, drill hole KA92-40 @ 862 m, **B)** Little River Formation-variably altered mafic volcanoclastic rocks with garnet-biotite \pm cordierite porphyroblasts, drill hole KA93-40 @ 578 m. Note: Dark-green colour is due to high content of chlorite in the unit, **C)** syngenetic stockwork vein of chalcopyrite-pyrrhotite- with a late-stage (post-S₄) quartz vein parallel to a S₁ fabric and locally folded in a chlorite-altered felsic tuff (Nepisiguit Falls formation), drill hole KA92-38 @ 682m, and **D)** magnetite-rich sedimentary rocks (Little River Formation) with garnet-biotite porphyroblasts. Sample is from drill hole KA92-42 @ 189.6 m. Note: garnets are concentrated within the phyllosilicate-rich layers. Samples are from the Key Anacon East Zone (Zulu, 2012). Scale in cm.

Figure 4. Zr/TiO₂ versus Nb/Y discrimination diagram for volcanic rocks from the study area. **A)** Key Anacon East Zone deposit: **B)** Key Anacon Main Zone (Zulu, 2012). Field boundaries in both diagrams are from Winchester and Floyd (1977).

Figure 5. High field strength element-based differentiation diagrams for volcanic rocks at the Key Anacon east and Key Anacon main zone: **A and B)** Zr versus TiO₂, **C and D)** TiO₂/Al₂O₃ versus Y/Al₂O₃.

Figure 6. Zr versus Al₂O₃ plot of metamorphosed altered rocks from the Key Anacon Main Zone. The line represents primary composition; samples above the line have undergone mass gain, whereas samples falling below the line have undergone mass loss (after Zulu, 2012). Samples are felsic volcanic rocks from drill hole KA92-10.

Figure 7. Down hole variation of major- and trace-element mass changes in drill hole KA92-10. These data illustrates intense footwall alteration characterized by mass addition of Fe₂O₃ (Total), MgO, Pb, Zn, Cu, and S^T, and mass loss of SiO₂, Na₂O, and K₂O relative to the precursor. The hanging wall Nepisiguit Falls formation (NF Fm) rocks have had addition of MnO, Sr, and CaO, and depletion of Na₂O, Rb, and SiO₂. Note that the overall structure is an overturned syncline with fold axis indicated.

Figure 8. Binary plots of selected major-element compositional change illustrating the relationships between geochemical variations and alteration mineral assemblage. **A)** ΔK_2O versus ΔNa_2O , **B)** ΔFe_2O_3 (Total) + ΔMgO versus ΔK_2O , **C)** ΔFe_2O_3 (Total) versus ΔK_2O , and **D)** ΔMgO versus ΔK_2O (Zulu, 2012). Samples are from the Key Anacon Main Zone (NF Fm).

Figure 9. A histogram of reconstructed mass for the metamorphosed hydrothermal altered felsic volcanic rocks (n=52) from the NF Fm of the Key Anacon Main Zone (Zulu, 2012). The least altered sample 19 is from drill hole KA92-5 @ 432.18 m.

Figure 10. Al_{major} versus Al_{trace} diagram showing the characteristic fields of the least-altered, sericitized, and chloritized volcanic rocks (NF Fm; after Zulu, 2012); samples are from the Key Anacon Main Zone (adapted from Häussinger et al., 1993).

Figure 11. Down hole plot of AI, GI (in log scale), and CCPI alteration indices for drill hole (KA92-10) at the Key Anacon Main Zone (see Table 3; Zulu, 2012). Note that the overall structure is an overturned syncline with the position of the fold axis indicated (Fig. 12; Zulu, 2012).

Figure 12. Geologic cross section through the Key Anacon Main Zone showing position of drill cores KA92-32 and KA92-10. Line of section A-A' is presented on Figure 2.

Figure 13. Molar Element Ratio plots of 51 samples (NF Fm) from the Key Anacon Main Zone stratigraphic hangingwall and footwall. **A)** Na/Al versus K/Al diagram showing the alteration minerals that control content of Na_2O and K_2O . **B)** Fe/Al versus Mg/Al discrimination diagram showing variations of Fe_2O_3 (Total) and MgO in the alteration zones (Zulu, 2012). Values of Fe and Mg-rich chlorite in **(B)** are from microprobe analyses in Appendix E (Zulu, 2012).

Figure 14. Molar Element Ratio plots of 51 samples (NF Fm) from the alteration zones of stratigraphic hanging wall and footwall. **A)** Fe/Al versus K/Al. **B)** Mg/Al versus K/Al. The plots illustrate the control of muscovite, Fe-rich chlorite, Mg-rich chlorite, and pyrite on compositional variation of Fe_2O_3 (Total), MgO, and K_2O . Values of Fe and Mg-rich chlorite are from microprobe analyses in Appendix E (Zulu, 2012).

Figure 15. Petrogenetic grid for altered felsic volcanic rocks (NF Fm) showing the modelled P - T for a chloritic and minor sericitic alteration. The peak assemblage of sample KA92-10 @ 726 m from the Key Anacon Main Zone is indicated by Ilm+Crd+Bt+Qtz (mineral abbreviations from Kretz, 1983).

Figure 16. Petrogenetic grid for altered felsic volcanic rocks (NF Fm) showing the modelled pressure-temperature for a sericitic alteration type. The peak assemblage of sample 94-DL-87 from the Key Anacon East Zone is indicated by Ilm=Grt+Chl+Phg+Bt (stage 2) Sample 94-DL-87 (from drill hole KA92-40 @ 669.2 m) comes from the immediate stratigraphic footwall rocks (NF Fm) to the massive sulfide deposits (Zulu, 2012). Stages 1 to 3 show progression of metamorphic grade. Mineral abbreviations from Kretz (1983).

List of Tables

TABLE 1. Representative whole-rock geochemistry data from the Key Anacon Main Deposits.

TABLE 1: COMPOSITIONAL CHANGES FOR CHEMOSTRATIGRAPHIC NF Fm IN THE KEY ANACON MAIN DEPOSITS.

TABLE 3. Al_{major} , Al_{trace} , AI, GI, AND CCPI FOR CHEMOSTRATIGRAPHIC NF Fm IN DRILL HOLE KA92-10, KEY ANACON MAIN ZONE DEPOSITS.

Figure 1.

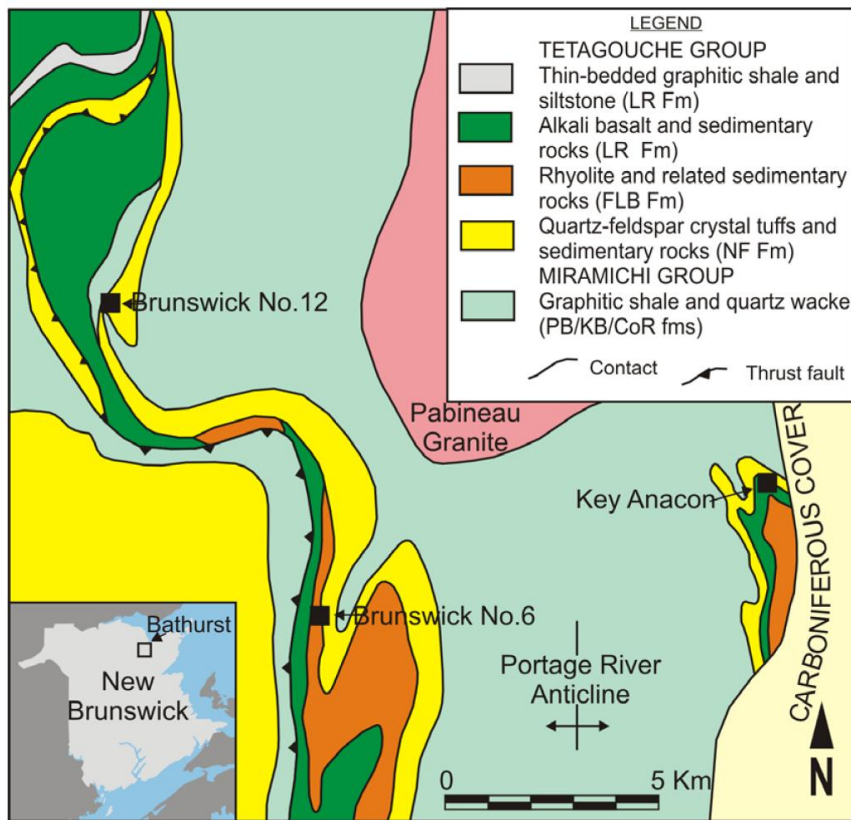
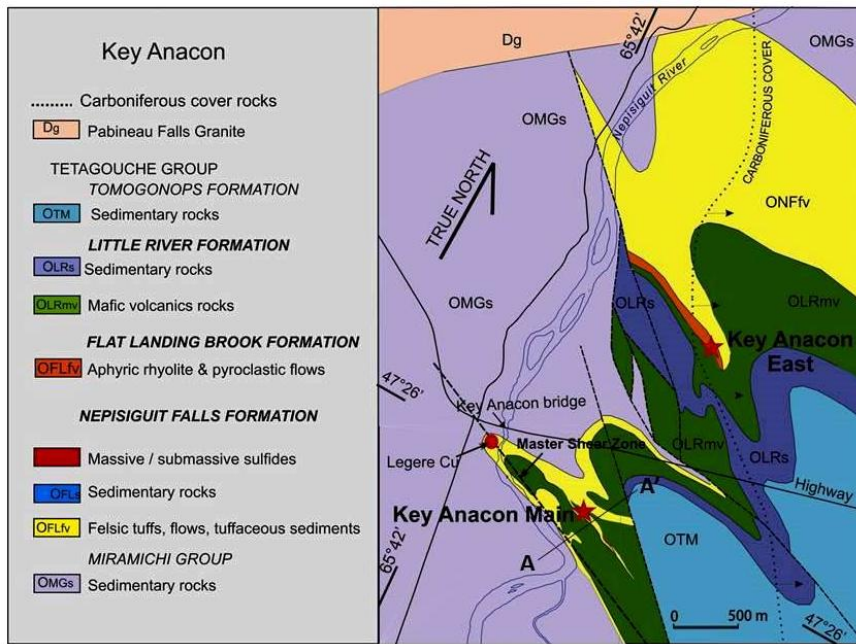


Figure 2.



ACCEPTED MANUSCRIPT

Figure 3.

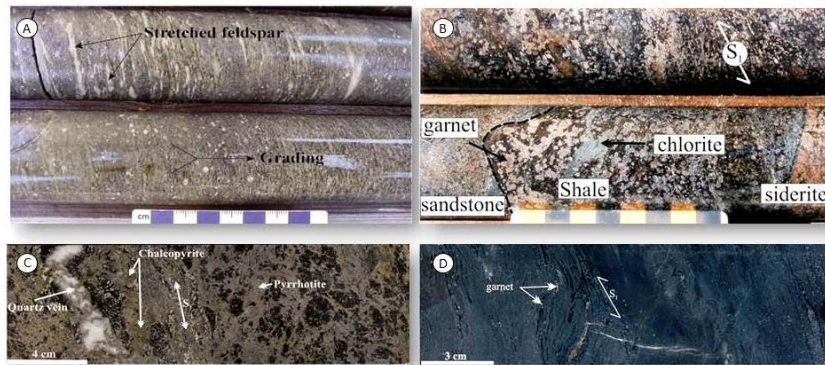


Figure 4.

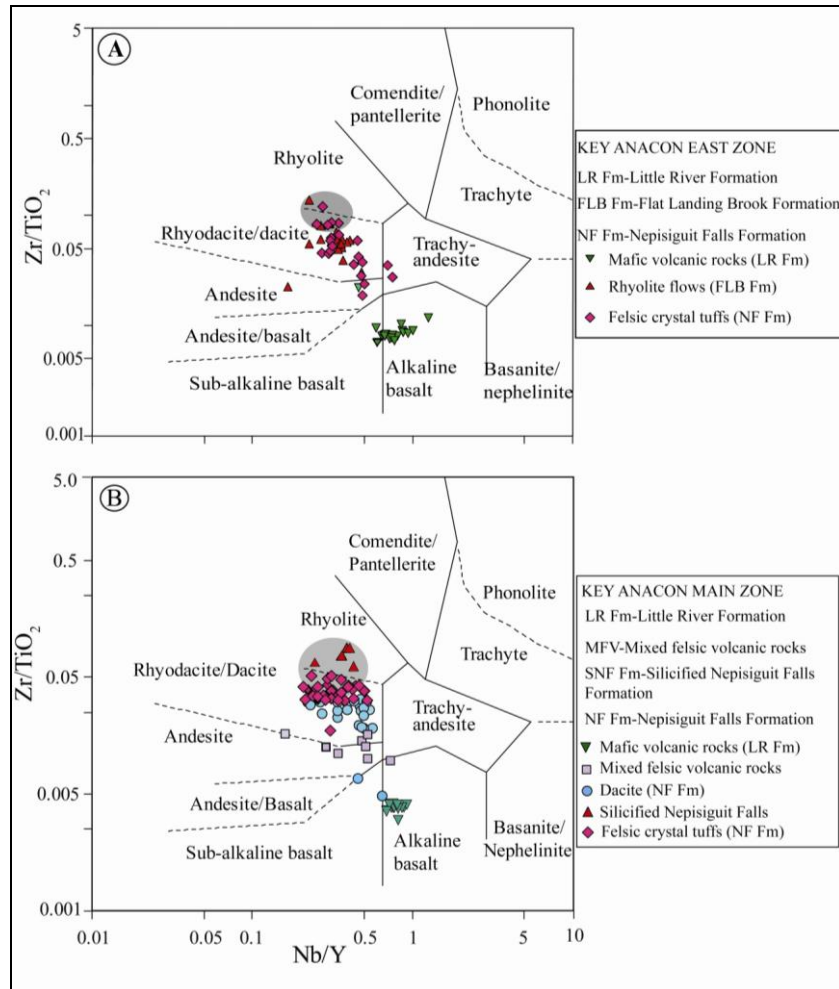


Figure 5.

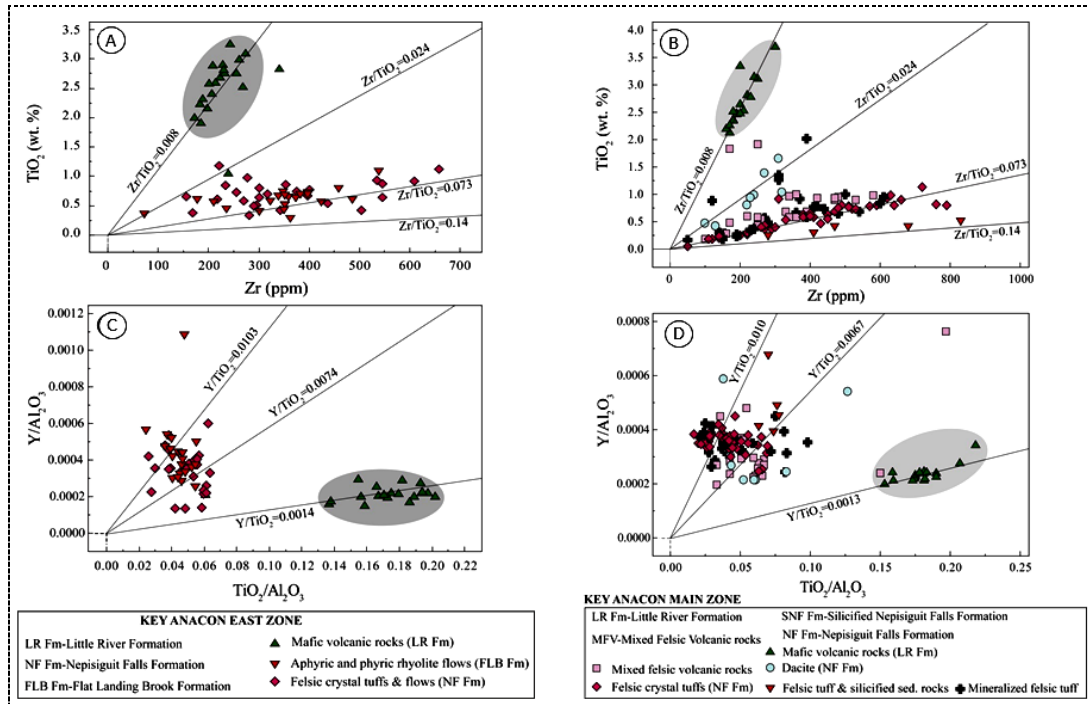


Figure 6.

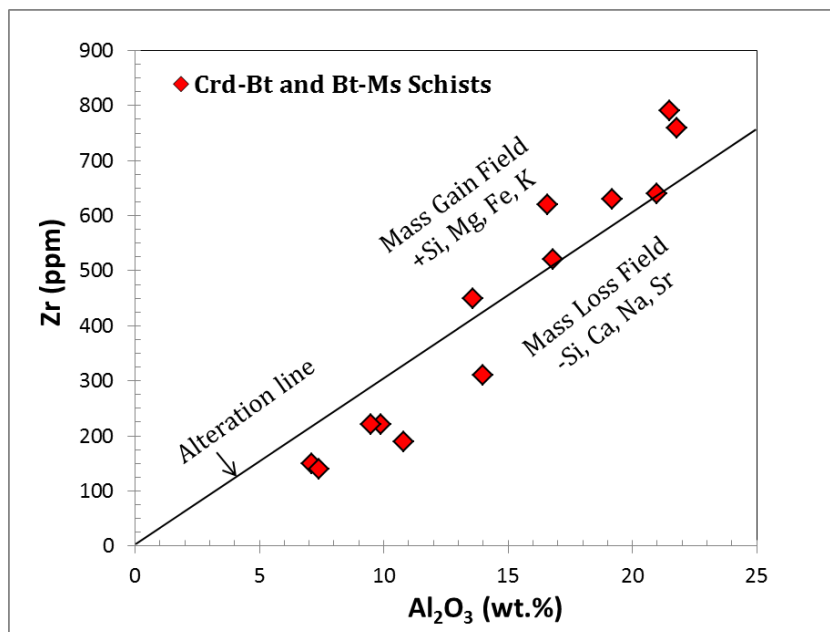


Figure 7.

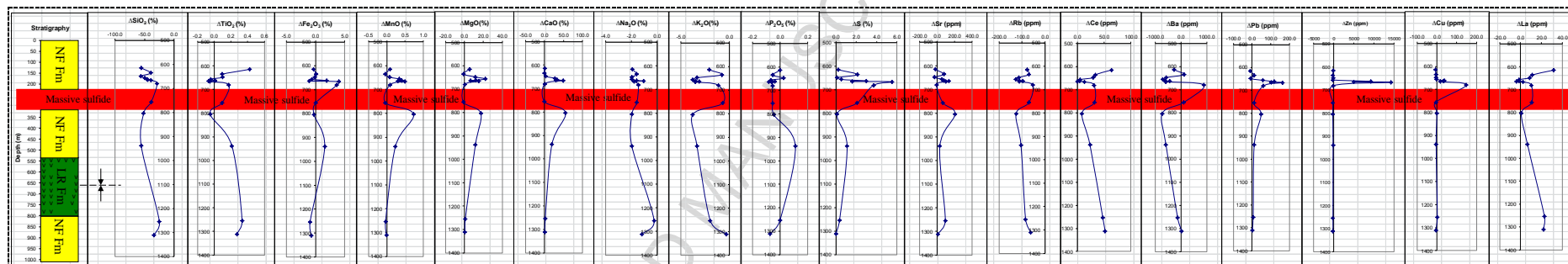


Figure 8.

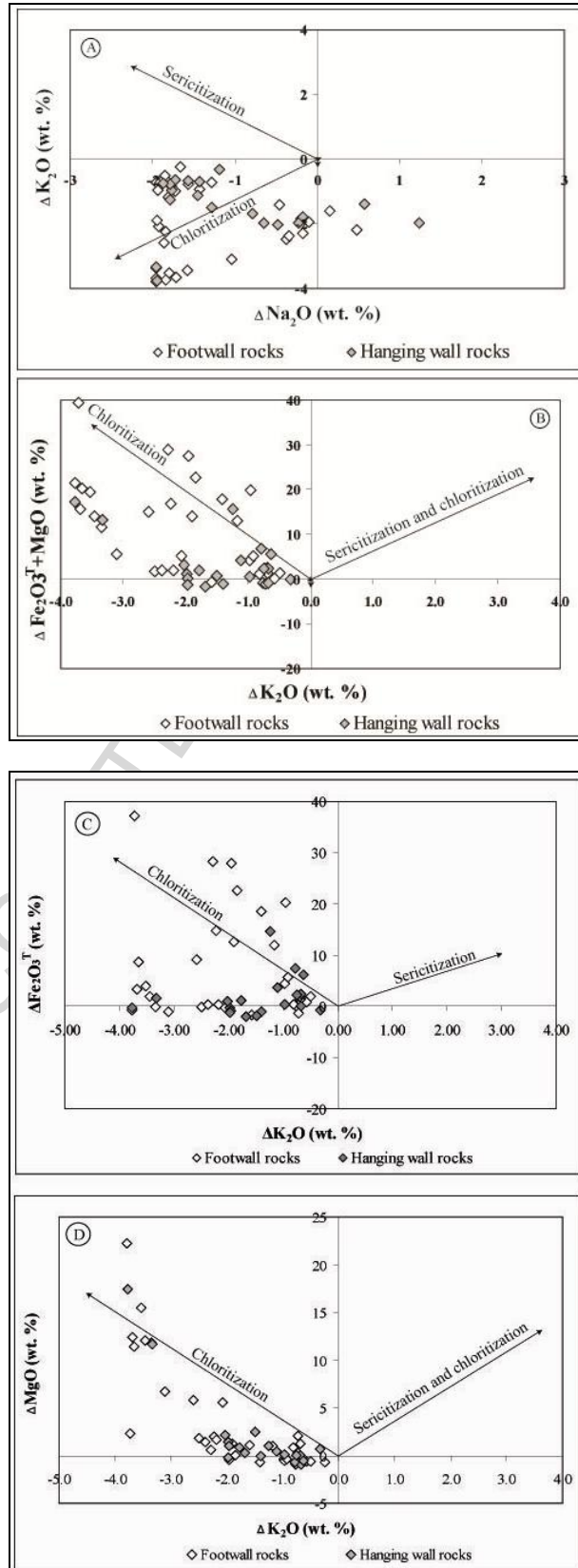


Figure 9.

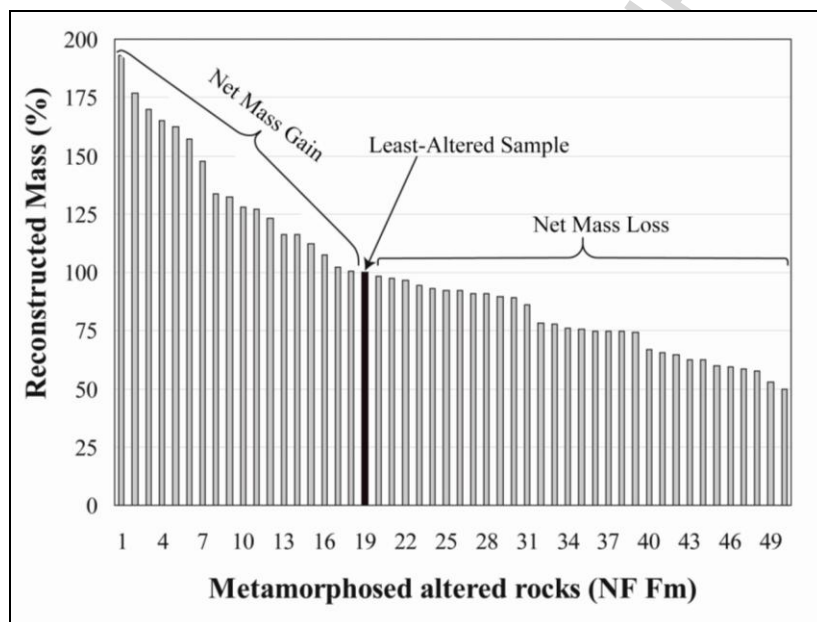


Figure 10.

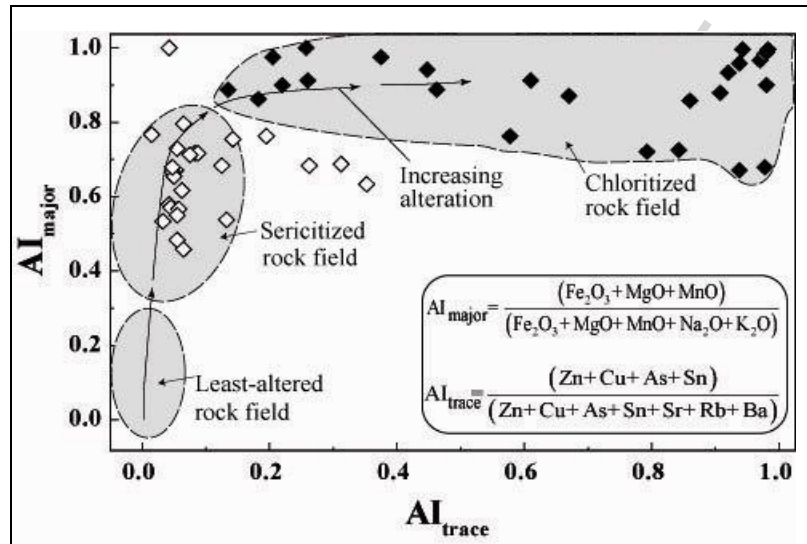


Figure 11.

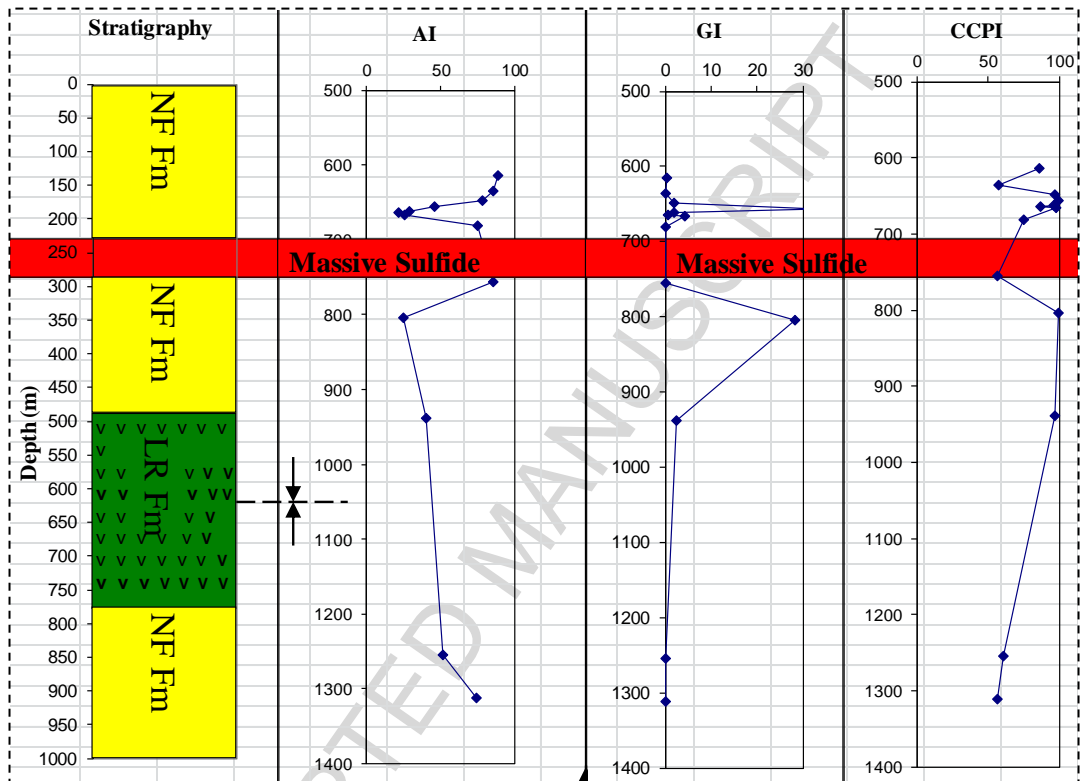


Figure 12.

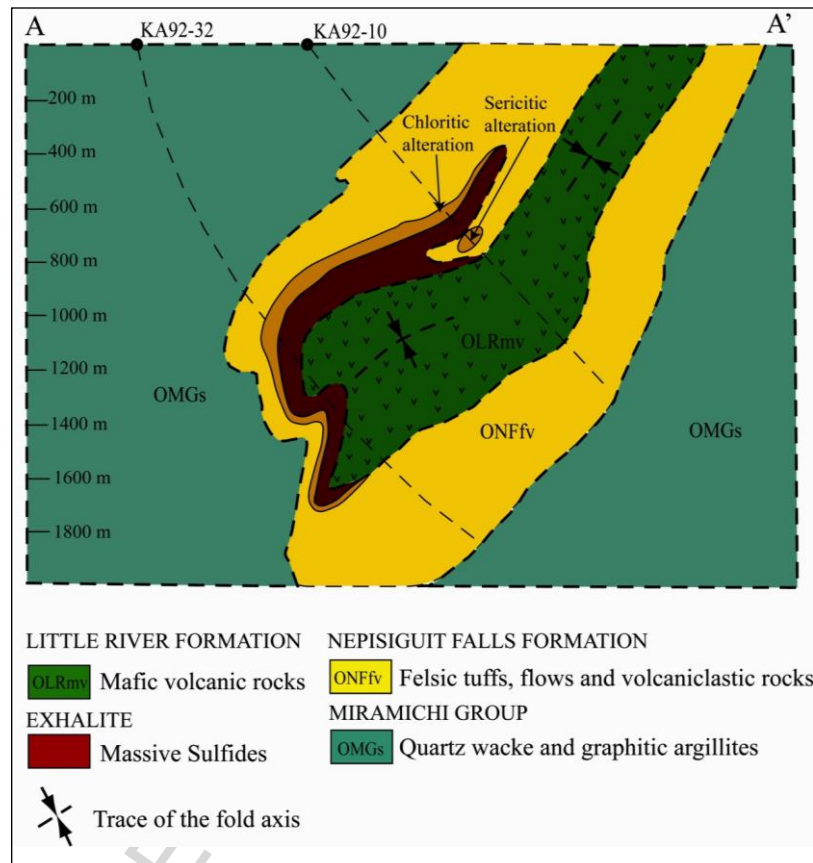


Figure 13.

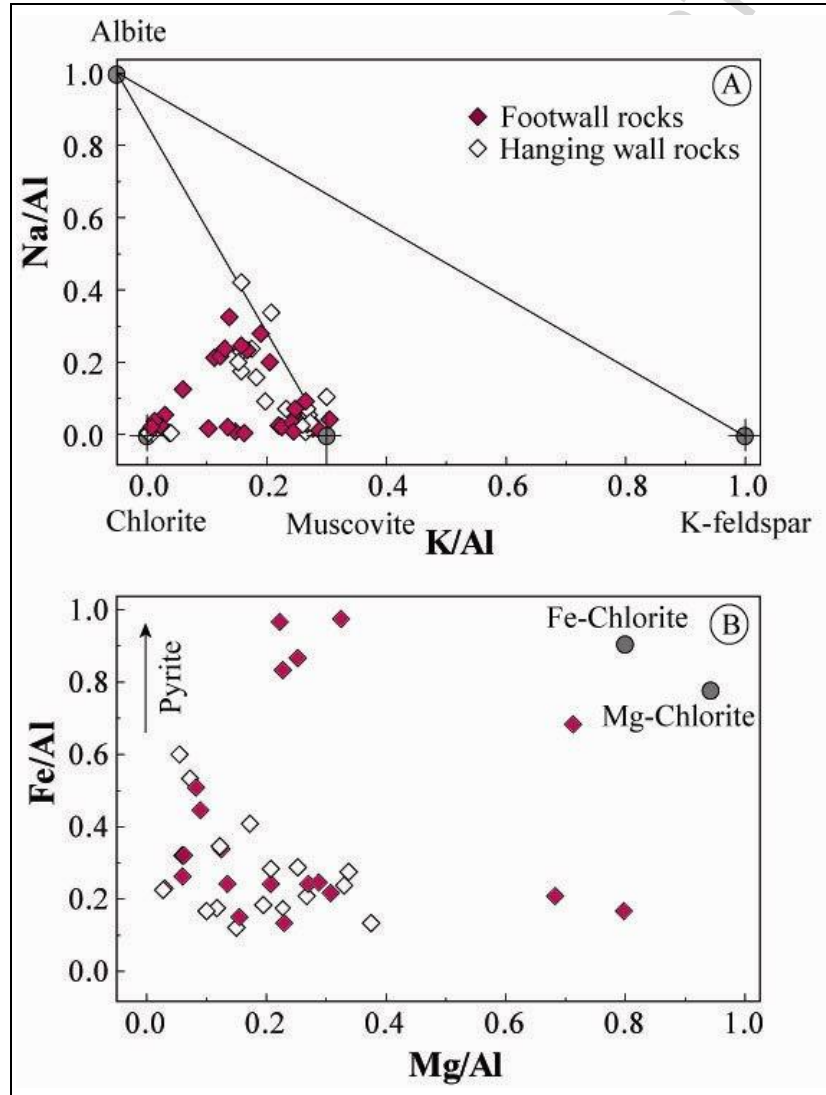


Figure 14.

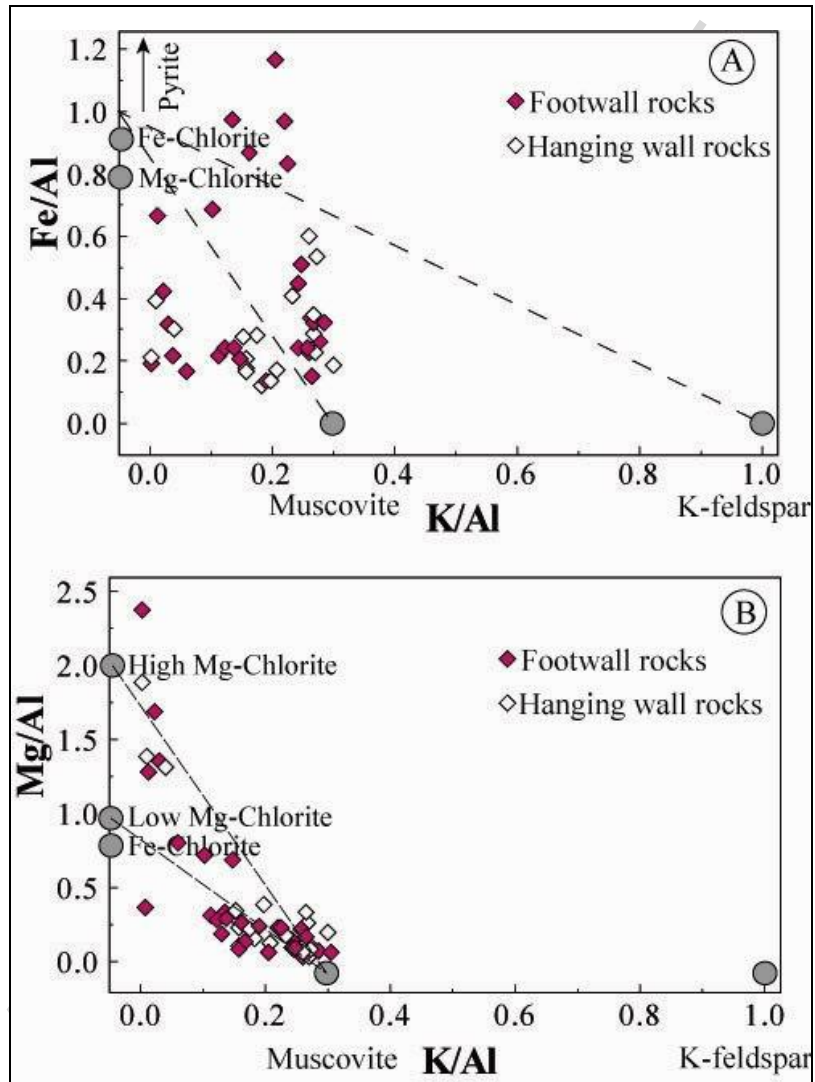


Figure 15.

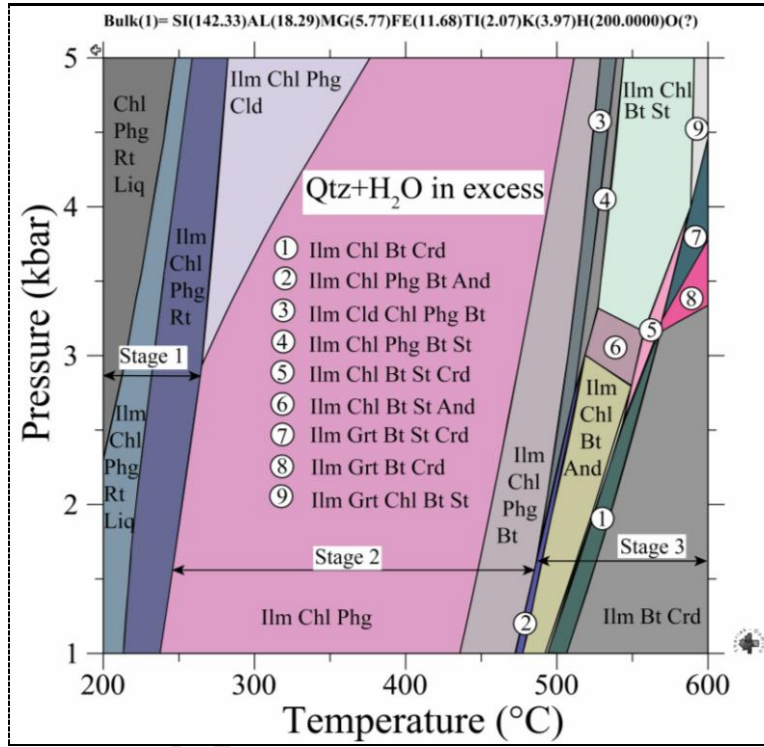


Figure 16.

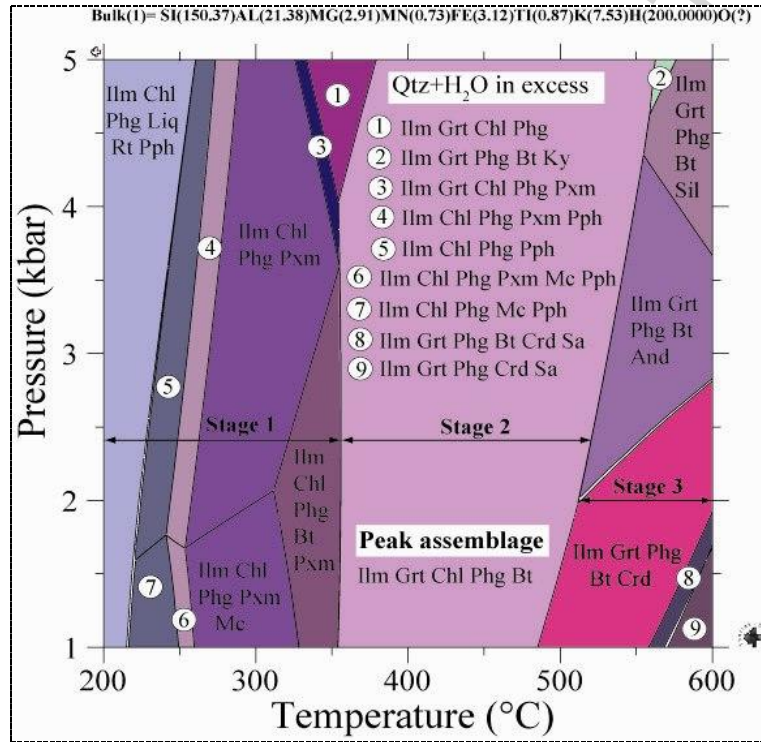


Table 1.

Felsic volcanic rocks (NF Fm)				KEY ANACON MAIN ZONE											
Sample	LPA-71	LPA-72	LPA-73	LPA-74	LPA-76	LPA-77	LPA-82	LPA-83	LPA-86	LPA-95	LPA-99	LPA-106	LPA-107	LPA-118	Avg
SiO ₂	83.20	77.70	74.60	26.80	75.60	69.30	66.40	70.00	62.90	77.60	71.20	62.80	63.40	76.00	68.39
TiO ₂	0.21	0.23	0.36	0.58	0.55	0.68	0.58	0.53	0.80	0.65	0.39	0.67	0.72	0.29	0.52
Al ₂ O ₃	7.60	10.80	12.80	9.80	8.00	9.40	13.80	14.10	16.80	10.20	5.60	16.50	16.20	13.00	11.76
Fe ₂ O ₃ t	3.80	5.40	4.80	10.20	10.40	14.30	3.70	3.60	7.40	7.10	11.00	5.50	6.10	2.70	6.86
MnO	0.02	0.01	0.05	0.64	0.12	0.22	0.06	0.04	0.05	0.05	0.02	0.14	0.09	0.02	0.11
MgO	0.37	0.55	2.12	9.90	1.44	2.43	1.29	1.12	2.77	0.74	0.33	4.01	3.48	2.38	2.35
CaO	0.52	0.07	0.11	19.70	0.11	0.07	4.12	2.06	2.16	0.12	0.06	3.26	2.40	0.83	2.54
Na ₂ O	0.10	0.10	0.20	0.20	0.10	0.10	2.80	3.60	2.40	0.20	0.02	2.10	2.10	2.20	1.16
K ₂ O	1.89	2.85	3.05	0.12	1.68	1.18	2.65	2.06	2.72	2.30	1.27	1.73	1.84	2.30	1.97
P ₂ O ₅	0.03	0.06	0.09	0.16	0.10	0.10	0.13	0.13	0.14	0.10	0.10	0.10	0.13	0.08	0.10
S(t)	2.34	2.88	2.14	4.22	4.38	3.05	0.37	0.24	2.75	1.88	4.76	2.19	3.46	1.07	2.55
Ce	43.00	62.00	84.00	95.00	64.00	74.00	91.00	91.00	130.00	67.00	48.00	120.00	130.0	68.0	83.36
Dy	4.50	6.20	7.10	5.60	4.40	5.40	7.90	8.80	9.90	4.50	3.50	10.00	9.70	7.60	6.79
Er	2.60	3.50	3.70	2.90	2.40	2.90	4.30	4.70	5.00	2.40	1.80	5.60	5.20	4.10	3.65
Eu	0.88	0.94	0.98	1.30	1.70	1.70	1.50	1.20	1.90	1.90	1.60	1.50	1.70	0.58	1.38
Gd	4.40	6.20	7.80	7.30	5.00	6.30	9.30	10.00	13.00	5.60	4.40	12.00	12.00	8.10	7.96
Ho	0.93	1.30	1.50	1.20	0.89	1.00	1.50	1.80	1.90	0.85	0.66	2.00	1.90	1.50	1.35
La	19.00	27.00	37.00	45.00	28.00	36.00	48.00	46.00	64.00	34.00	24.00	59.00	62.00	32.00	40.07
Lu	0.40	0.55	0.57	0.47	0.40	0.53	0.66	0.70	0.79	0.42	0.31	0.85	0.80	0.56	0.57
Nd	20.00	29.00	39.00	43.00	28.00	34.00	45.00	46.00	63.00	31.00	22.00	55.00	59.00	33.00	39.07
Pr	5.10	7.50	10.00	11.00	7.30	9.40	12.00	12.00	17.00	8.60	6.10	15.00	16.00	9.00	10.43
Sm	4.40	6.40	8.20	7.70	5.50	6.70	9.00	9.70	13.00	6.10	4.40	12.00	12.00	7.50	8.04
Tb	0.77	1.10	1.30	1.10	0.81	0.93	1.40	1.50	1.80	0.81	0.62	1.70	1.70	1.30	1.20
Tm	0.44	0.60	0.68	0.50	0.43	0.51	0.68	0.77	0.81	0.41	0.31	0.92	0.83	0.66	0.61
Y	28.00	40.00	43.00	34.00	25.00	30.00	47.00	52.00	55.00	25.00	19.00	60.00	57.00	45.00	40.00
Yb	2.70	3.60	3.80	3.00	2.60	3.30	4.30	4.70	5.10	2.60	1.90	5.70	5.10	4.00	3.74
Ag	2.40	4.10	0.60	6.80	0.50	0.30	0.05	0.10	0.20	0.20	4.80	0.10	0.10	0.05	1.45

Ba	130.00	200.00	280.00	30.00	100.00	90.00	570.00	690.00	730.00	220.00	120.00	270.00	390	470	306.43
Be	1.90	2.10	3.50	5.40	5.40	6.40	5.40	5.10	7.50	6.00	3.60	6.40	6.80	2.80	4.88
Co	2.50	7.00	2.50	2.50	21.00	18.00	5.00	10.00	9.00	9.00	28.00	5.00	5.00	2.50	9.07
Cu	49.00	100.00	30.00	27.00	340.00	120.00	11.00	22.00	16.00	440.00	10000.00	5.00	5.00	5.00	797.86
Cr	120.00	110.00	74.00	26.00	120.00	74.00	41.00	60.00	70.00	130.00	230.00	130.00	99.00	54.00	95.57
Ni	5.00	40.00	5.00	10.00	20.00	19.00	20.00	40.00	24.00	17.00	16.00	5.00	5.00	5.00	16.50
Sc	6.30	3.90	5.90	7.50	7.40	8.50	10.00	10.00	15.00	9.30	5.70	10.00	10.00	4.00	8.11
Sr	10.00	23.00	10.00	67.00	21.00	10.00	160.00	150.00	210.00	10.00	10.00	220.00	240.0	130.0	90.79
Zn	9600.00	4800.00	110.00	5500.00	46.00	1600.00	39.00	44.00	36.00	14.00	10.00	49.00	52	18	1565.57
V	2.50	2.50	2.50	20.00	36.00	47.00	16.00	12.00	37.00	41.00	19.00	14.00	21.00	2.50	19.50
Cs	1.60	2.60	2.90	0.28	1.40	1.00	4.90	2.30	2.10	2.90	1.80	3.90	2.70	1.80	2.30
Ga	9.80	14.00	17.00	13.00	11.00	12.00	19.00	19.00	23.00	15.00	8.30	22.00	22.00	16.00	15.79
Hf	3.90	4.90	7.00	9.70	10.00	12.00	8.50	8.30	12.00	8.70	6.30	12.00	12.00	5.70	8.64
Mo	1.10	9.80	1.50	1.30	1.80	1.50	0.50	0.20	6.80	0.90	1.60	2.40	2.20	2.00	2.40
Nb	6.30	8.10	11.00	13.00	11.00	14.00	14.00	15.00	19.00	13.00	8.10	18.00	18.00	10.00	12.75
Pb	100.00	100.00	59.00	100.00	18.00	49.00	21.00	23.00	31.00	8.00	7.00	37.00	24.00	11.00	42.00
Rb	77.00	100.00	100.00	4.50	68.00	48.00	100.00	83.00	60.00	100.00	62.00	65.00	67.0	57.0	70.82
Ta	0.70	1.20	1.20	1.20	0.90	1.10	1.00	0.90	1.10	1.30	0.70	1.50	1.30	0.90	1.07
Th	10.00	15.00	18.00	16.00	11.00	13.00	17.00	18.00	24.00	11.00	7.70	24.00	23.00	17.00	16.05
Tl	3.70	4.80	4.60	0.29	11.00	3.80	0.60	0.53	0.72	3.50	0.80	1.20	1.80	0.85	2.73
U	2.50	3.80	4.30	2.30	2.30	3.00	4.10	4.80	4.90	2.80	1.80	5.70	5.10	5.00	3.74
Zr	150.00	190.00	290.00	390.00	450.00	540.00	380.00	330.00	490.00	400.00	300.00	470.00	530.0	220.0	366.43

Table 2.

Sample No	Drill Hole	Depth (m)	ΔSiO_2	ΔTiO_2	$\Delta\text{Al}_2\text{O}_3$	$\Delta\text{Fe}_2\text{O}_3$	ΔMnO	ΔMgO	ΔCaO	$\Delta\text{Na}_2\text{O}$	$\Delta\text{K}_2\text{O}$	$\Delta\text{P}_2\text{O}_5$	$\Delta\text{S(t)}$	ΔCe	ΔDy
93-LPA-33	KA92-10	615	55.67	0.42	0.00	-0.30	0.09	5.54	0.54	1.92	2.07	0.00	0.22	63.70	2.78
93-LPA-34	KA92-10	635	39.68	0.10	0.00	0.10	0.04	0.94	0.27	1.56	0.77	-0.05	2.12	33.42	3.48
93-LPA-35	KA92-10	648	56.69	0.10	0.00	-0.09	0.08	11.80	3.31	1.96	3.35	0.03	0.13	29.81	2.48
93-LPA-37	KA92-10	656	50.09	-0.04	0.00	-0.66	0.34	22.23	26.95	1.95	3.78	-0.07	0.52	5.16	2.53
93-LPA-38	KA92-10	662	46.19	0.01	0.00	1.87	0.41	12.11	33.26	1.57	3.45	-0.04	2.99	4.18	4.03
93-LPA-39	KA92-10	664	44.60	-0.07	0.00	-1.08	0.30	6.69	30.14	1.04	3.10	-0.08	1.59	0.40	3.21
93-LPA-41	KA92-10	666	39.24	-0.05	0.00	3.97	0.50	15.48	49.44	1.79	3.53	-0.06	5.51	13.72	3.79
93-LPA-43	KA92-10	681	29.00	0.18	0.00	3.66	0.08	0.49	0.48	1.45	1.11	-0.06	3.70	31.30	2.18
93-LPA-51	KA92-10	755	38.82	0.10	0.00	0.04	0.04	0.96	0.26	1.57	0.68	-0.06	2.10	32.05	3.94
93-LPA-52	KA92-10	804	51.66	-0.05	0.00	-0.27	0.73	17.43	55.22	1.94	3.77	-0.05	0.12	8.79	2.26
93-LPA-54	KA92-10	939	55.83	0.21	0.00	1.57	0.24	11.69	19.31	1.96	3.33	0.11	1.11	23.69	4.17
93-LPA-58	KA93-10	1255	25.06	0.33	0.00	-0.94	0.03	1.03	1.65	0.23	1.96	0.00	0.36	47.60	2.87
93-LPA-61	KA93-10	1312	34.18	0.27	0.00	-0.74	0.01	0.70	0.62	1.19	0.32	-0.07	0.00	51.86	2.50
Sample No	Drill Hole	Depth (m)	ΔEr	ΔEu	ΔGd	ΔHo	ΔLa	ΔLu	ΔNd	ΔPr	ΔSm	ΔTb	ΔTm	ΔY	ΔYb

93-LPA-33	KA92-10	615	1.24	0.39	4.02	0.63	31.80	0.42	28.85	7.78	4.70	0.45	0.27	0.86	-38.02
93-LPA-34	KA92-10	635	1.95	0.33	3.90	0.88	11.41	0.47	15.77	4.60	3.66	0.55	0.37	6.49	-37.35
93-LPA-35	KA92-10	648	1.58	0.12	2.33	0.69	8.88	0.49	11.50	3.10	2.10	0.35	0.33	1.06	-37.59
93-LPA-37	KA92-10	656	1.26	-0.21	1.78	0.65	-1.27	0.37	0.76	0.70	0.96	0.39	0.24	0.13	-38.20
93-LPA-38	KA92-10	662	1.81	0.35	2.88	0.98	-1.26	0.38	0.77	0.66	1.27	0.60	0.30	9.56	-37.90
93-LPA-39	KA92-10	664	1.75	0.32	1.88	0.76	-3.92	0.42	0.72	0.24	0.59	0.43	0.32	6.84	-37.84
93-LPA-41	KA92-10	666	2.23	0.54	3.57	1.08	2.39	0.46	6.19	1.88	2.58	0.58	0.36	11.07	-37.48
93-LPA-43	KA92-10	681	0.89	0.68	2.77	0.48	10.37	0.29	12.40	3.54	2.70	0.42	0.17	4.62	-38.82
93-LPA-51	KA92-10	755	2.06	0.25	3.77	0.92	10.80	0.46	17.44	4.43	4.10	0.65	0.36	8.70	-37.31
93-LPA-52	KA92-10	804	1.18	1.08	2.02	0.59	0.96	0.31	2.99	0.99	1.03	0.39	0.20	2.13	-38.53
93-LPA-54	KA92-10	939	2.53	0.52	3.32	0.98	6.72	0.59	11.52	3.41	2.23	0.63	0.50	14.34	-36.81
93-LPA-58	KA93-10	1255	1.69	0.63	3.63	0.72	23.00	0.42	23.52	5.95	3.57	0.59	0.37	5.67	-38.02
93-LPA-61	KA93-10	1312	1.38	0.35	4.36	0.63	21.96	0.38	23.99	6.07	4.20	0.59	0.32	2.48	-38.27
Sample No	Drill Hole	Depth (m)	Δ Ag	Δ Ba	Δ Be	Δ Co	Δ Cu	Δ Cr	Δ Ni	Δ Sc	Δ Sr	Δ Zn	Δ V	Δ Cs	Δ Ga
93-LPA-33	KA92-10	615	-0.05	-263.56	4.64	0.49	-5.51	8.92	-5.51	7.46	-21.09	-127.40	5.37	-1.05	3.44
93-LPA-	KA92-	635	0.15	124.2	1.29	-1.08	-	11.6	-5.0	6.68	78.5	-	-26.8	-0.5	2.53

34	10			8			5.08	3	8		2	206.43	2	7	
93-LPA-35	KA92-10	648	-0.08	572.57	1.22	-1.01	5.01	3.24	5.01	3.97	30.26	126.40	28.42	1.99	1.75
93-LPA-37	KA92-10	656	0.05	701.25	0.16	-0.83	1.66	5.84	1.66	2.23	55.30	203.79	31.83	1.91	2.76
93-LPA-38	KA92-10	662	6.67	619.79	0.24	-0.69	36.95	14.73	1.39	2.27	82.21	9267.16	31.69	1.17	0.87
93-LPA-39	KA92-10	664	3.87	438.00	0.62	-1.09	32.70	3.93	2.19	1.28	136.07	4981.33	32.09	0.17	0.12
93-LPA-41	KA92-10	666	10.41	592.79	0.50	0.42	18.54	16.61	0.85	1.01	98.60	14253.92	30.58	1.60	1.45
93-LPA-43	KA92-10	681	0.47	892.76	1.90	6.47	149.00	42.06	4.26	8.46	-2.90	109.95	18.55	0.17	0.70
93-LPA-51	KA92-10	755	0.15	112.22	1.22	-1.12	5.12	11.23	5.12	6.52	65.23	205.91	25.78	0.65	2.28
93-LPA-52	KA92-10	804	0.03	726.54	0.61	0.24	0.49	5.06	0.49	1.28	204.59	247.76	30.76	2.00	3.67
93-LPA-54	KA92-10	939	0.17	576.53	2.12	1.54	3.38	17.17	70.50	5.16	32.19	183.66	24.84	1.27	2.55
93-LPA-58	KA93-10	1255	0.03	124.00	3.56	2.81	2.59	48.83	0.43	7.11	93.76	206.60	4.73	1.09	2.40
93-LPA-61	KA93-10	1312	0.07	33.00	2.82	1.89	4.73	34.68	0.15	6.78	10.18	197.70	4.25	0.99	2.01

Sample No	Drill Hole	Depth (m)	ΔH_f	ΔM_o	ΔN_b	ΔP_b	ΔR_b	ΔT_a	ΔT_h	ΔT_l	ΔU	ΔZ_r
93-LPA-33	KA92-10	615	8.08	3.38	7.94	-9.51	-77.16	0.57	9.91	1.42	1.17	466.94
93-LPA-34	KA92-10	635	5.05	5.51	3.19	10.54	-68.58	0.04	3.75	9.16	1.95	280.51
93-LPA-35	KA92-10	648	4.69	8.07	5.34	-8.02	-113.84	0.42	4.13	2.46	4.71	201.78
93-LPA-37	KA92-10	656	2.48	5.86	0.43	57.05	-126.37	0.23	1.94	-0.71	1.29	98.11
93-LPA-38	KA92-10	662	2.79	4.19	0.96	118.21	-111.13	0.28	2.52	2.27	2.29	109.86
93-LPA-39	KA92-10	664	1.17	2.80	-1.65	102.30	-95.60	0.03	0.77	4.81	2.15	39.96

93-LPA-41	KA92-10	666	2.02	4.69	-0.15	162.90	-112.32	0.10	1.25	2.59	2.53	84.35
93-LPA-43	KA92-10	681	4.09	0.29	1.46	60.76	-52.24	0.27	4.43	11.19	0.45	207.76
93-LPA-51	KA92-10	755	4.91	5.41	2.98	10.77	-69.39	0.26	2.96	9.60	1.76	256.87
93-LPA-52	KA92-10	804	0.89	6.31	-1.99	48.80	-125.64	-0.10	2.75	-0.53	1.43	56.62
93-LPA-54	KA92-10	939	5.28	32.67	5.55	11.86	-103.91	0.61	4.60	2.65	11.12	234.59
93-LPA-58	KA93-10	1255	5.71	-0.74	3.89	6.43	-83.87	0.35	6.90	-0.29	-0.48	288.11
93-LPA-61	KA93-10	1312	4.28	-1.30	2.39	1.70	-61.58	0.40	8.26	-0.59	-2.02	231.13

Table 3.

DDH No	Sample No	Depth	Almajor	Altrace	AI	GI	CCPI
KA92-5	93-LPA-03	333.97	0.72	0.08	96.27	0.27	71.37
KA92-5	93-LPA-06	391.35	0.89	0.14	91.21	0.51	88.54
KA92-5	93-LPA-07	396.42	0.67	0.05	83.87	0.21	66.52
KA92-5	93-LPA-08	402.50	0.94	0.45	95.95	0.97	93.94
KA92-5	93-LPA-09	409.67	0.63	0.35	94.25	0.23	63.13
KA92-5	93-LPA-11	431.68	0.99	0.98	63.15	9.82	99.37
KA92-5	93-LPA-12	454.80	0.72	0.79	96.14	0.25	71.76
KA92-5	93-LPA-13	462.80	0.72	0.84	84.73	0.28	71.87
KA92-4	93-LPA-21	363.81	0.68	0.13	60.56	0.26	68.07
KA92-4	93-LPA-22	407.73	0.54	0.13	59.94	0.15	53.50
KA92-10	93-LPA-33	614.61	0.86	0.18	89.10	0.37	85.80
KA92-10	93-LPA-34	635.20	0.58	0.04	85.14	0.15	57.88
KA92-10	93-LPA-35	648.13	0.97	0.38	78.19	1.86	97.36
KA92-10	93-LPA-37	655.99	1.00	0.26	46.15	33.26	99.81
KA92-10	93-LPA-38	661.98	0.96	0.97	28.67	2.05	96.29
KA92-10	93-LPA-39	664.03	0.88	0.91	21.52	0.70	87.22
KA92-10	93-LPA-41	666.07	0.98	0.98	25.35	4.43	98.20
KA92-10	93-LPA-43	680.66	0.75	0.14	75.22	0.26	75.12
KA92-10	93-LPA-51	755.49	0.57	0.05	85.18	0.15	56.82
KA92-10	93-LPA-52	803.83	1.00	0.04	25.15	28.18	99.70
KA92-10	93-LPA-54	938.51	0.97	0.21	40.41	2.45	97.44
KA93-10	93-LPA-58	1254.50	0.61	0.06	51.71	0.18	61.27
KA93-10	93-LPA-61	1311.50	0.57	0.06	74.55	0.14	56.44
KA92-17	93-LPA-63	261.20	0.91	0.61	92.45	0.86	91.01
KA92-17	93-LPA-71	491.87	0.68	0.98	78.47	0.31	67.69
KA92-17	93-LPA-72	495.87	0.67	0.94	95.24	0.26	66.85

KA92-17	93-LPA-73	511.87	0.68	0.26	94.34	0.26	68.04
KA92-17	93-LPA-74	523.73	0.98	0.98	33.49	4.07	98.43
KA92-17	93-LPA-76	587.38	0.87	0.67	93.69	0.60	86.93
KA92-17	93-LPA-77	592.13	0.93	0.92	95.50	0.96	92.89
KA92-19	93-LPA-82	189.35	0.48	0.06	36.28	0.13	47.80
KA92-19	93-LPA-83	204.00	0.46	0.07	35.97	0.12	45.47
KA92-23	93-LPA-86	181.16	0.67	0.05	54.63	0.20	66.51
KA92-25	93-LPA-95	59.50	0.76	0.58	90.48	0.36	75.82
KA92-25	93-LPA-99	165.74	0.90	0.98	95.52	0.82	89.81
KA92-26	93-LPA-106	186.50	0.72	0.09	51.71	0.26	71.29
KA92-26	93-LPA-107	191.50	0.71	0.08	54.18	0.25	70.86
KA92-26	93-LPA-118	706.76	0.53	0.03	60.70	0.16	53.03
KA92-26	93-LPA-119	773.35	0.65	0.05	42.93	0.18	65.18
KA92-26	93-LPA-121	805.35	0.73	0.06	65.25	0.24	72.78
KA93-32	93-LPA-131	998.50	0.68	0.05	80.53	0.25	67.77
KA93-32	93-LPA-132	1006.36	0.69	0.31	78.86	0.17	68.55
KA93-32	93-LPA-133	1009.43	0.77	0.02	77.95	0.22	76.49
KA93-32	93-LPA-134	1010.41	0.79	0.07	74.63	0.26	79.30
KA92-2	93-LPA-153	680.20	0.76	0.20	87.21	0.28	75.91
KA92-2	93-LPA-155	862.00	0.91	0.26	57.86	0.73	91.21
KA92-2	93-LPA-156	866.65	0.88	0.46	57.14	0.64	88.32
KA92-2	93-LPA-157	875.00	0.86	0.86	60.11	0.33	85.65
KA92-2	93-LPA-159	939.50	0.90	0.22	48.95	0.57	89.90
KA92-2	93-LPA-163	1000.50	1.00	0.94	89.69	8.02	99.50
KA92-2	93-LPA-165	1041.61	0.95	0.94	74.02	1.43	95.48
KA92-18	93-LPA-167	52.73	0.55	0.06	54.96	0.14	54.35

Table 4.

ROCK UNIT	MG					
Sample No.	BR11-670 m					
Analysis	Core	Annulus 1	Annulus 2	Annulus 3	Annulus 4	Rim
SiO ₂	35.66	36.09	35.86	36.08	35.67	36.02
Al ₂ O ₃	20.11	20.22	20.30	20.31	20.28	20.26
TiO ₂	0.11	0.15	0.07	0.09	0.07	0.05
Cr ₂ O ₃	0.00	0.00	0.00	0.00	0.00	0.00
Sc ₂ O ₃	0.03	0.09	0.02	0.04	0.01	0.01
Y ₂ O ₃	0.98	0.00	0.00	0.00	0.00	0.00
FeO	16.52	19.96	28.05	33.56	38.66	38.90
MnO	20.38	16.74	12.18	7.24	3.16	2.98
MgO	0.38	0.33	0.72	1.16	1.52	1.38
CaO	3.95	5.61	2.24	1.56	0.45	0.38
Total	98.1	99.2	99.4	100.0	99.8	100.0
Si	5.95	5.92	5.91	5.91	5.86	5.91
Al	0.05	0.08	0.09	0.09	0.14	0.09
Al	3.91	3.83	3.85	3.83	3.79	3.83
Ti	0.01	0.02	0.01	0.01	0.01	0.01
Cr	0.00	0.00	0.00	0.00	0.00	0.00
Sc	0.01	0.01	0.00	0.01	0.00	0.00
Fe ³⁺	0.02	0.19	0.22	0.24	0.33	0.24
Y	0.09	0.00	0.00	0.00	0.00	0.00
Fe ²⁺	2.28	2.54	3.65	4.36	4.98	5.10
Mn	2.88	2.33	1.70	1.00	0.44	0.41
Mg	0.10	0.08	0.18	0.28	0.37	0.34
Ca	0.71	0.99	0.39	0.27	0.08	0.07
Total	16.0	16.0	16.0	16.0	16.0	16.0
X _{Alm}	38.2	41.5	59.4	70.8	80.2	82.8
X _{Sps}	48.1	37.9	27.7	16.3	7.1	6.7
X _{Prp}	1.6	1.3	2.9	4.6	6.0	5.5

X_{Grs}	11.8	16.1	6.4	4.4	1.3	1.1
Fe/(Fe+Mg)	0.96	0.97	0.95	0.94	0.93	0.94
Mg/(Mg+Fe)	0.040	0.031	0.046	0.061	0.070	0.062

Note: Mole fractions of Almandine (X_{Alm}), spessartine (X_{Sps}), pyrope (X_{Prp}), and grossular (X_{Grs}) are average ($n = 3$ for the core and annulus, $n = 4$ for the rims) mole % fractions of garnet porphyroblasts. All analyses are in units of wt. % and the calculated ions in atom percent per formula unit (apfu).

Highlights

Recognizing and quantifying metamorphosed alteration zones through amphibolite facies metamorphic overprint at the Key Anacon Zn-Pb-Cu-Ag deposits, Bathurst Mining Camp, New Brunswick, Canada.

Joseph D.S. Zulu¹, David R. Lentz¹, James A. Walker² and Christopher R.M. McFarlane¹

- We determined lithogeochemical alteration indices in metamorphosed base metal ores.
- Compositional change has been used to determine mass-loses and gains during the pre-metamorphic hydrothermal alteration related to deposit formation.
- The metamorphic assemblages of altered felsic volcanic rocks can be used as vectors or exploration guides to metamorphosed ores.



DSPACE

<https://dspace.org/>

Recognizing and quantifying metamorphosed alteration zones through amphibolite facies metamorphic overprint at the Key Anacon Zn-Pb-Cu-Ag deposits, Bathurst Mining Camp, New Brunswick, Canada

Zulu, Joseph D.S.; Lentz, David R.; Walker, James A.; McFarlane, Christopher R. M.

June 2016

Elsevier

<https://unbscholar.lib.unb.ca/handle/1882/22346>